J|A|C|S
ARTICLES

Published on Web 03/29/2010

Solid-State ^{115}In and ^{31}P NMR Studies of Triarylphosphine Indium Trihalide Adducts

Fu Chen, Guibin Ma, Guy M. Bernard, Ronald G. Cavell, Robert McDonald, Michael J. Ferguson, and Roderick E. Wasylishen*

Department of Chemistry, Gunning/Lemieux Chemistry Centre, University of Alberta, Edmonton, Alberta, Canada T6G 2G2

Received January 23, 2010; E-mail: Roderick.Wasylishen@ualberta.ca

Abstract: Solid-state ^{115}In and ^{31}P NMR spectroscopy, relativistic density functional theory (DFT) calculations, and single-crystal X-ray diffraction were used to investigate a series of triarylphosphine indium(III) trihalide adducts, $X_3In(PR_3)$ and $X_3In(PR_3)_2$ (X = Cl, Br or I; PR_3 = triarylphosphine ligand). The electric field gradient tensors at indium as well as the indium and phosphorus magnetic shielding tensors and the direct and indirect ^{115}In−^{31}P spin−spin coupling were characterized; for complexes possessing a C_3 symmetry axis, the anisotropy in the indirect spin−spin coupling, $\Delta J(^{115}In,^{31}P)$, was also determined. The ^{115}In quadrupolar coupling constants, $C_Q(^{115}In)$, range from $\pm 1.25 \pm 0.10$ to -166.0 ± 2.0 MHz. For any given phosphine ligand, the indium nuclei are most shielded for X = I and least shielded for X = Cl, a trend also observed for other group-13 nuclei in M(III) complexes. This experimental trend, attributed to spin−orbit effects of the halogen ligands, is reproduced by the DFT calculations. The spans of the indium magnetic shielding tensors for these complexes, $\delta_{11} - \delta_{33}$, range from 40 ± 7 to 710 ± 60 ppm; those determined for phosphorus range from 28 ± 1.5 to 50 ± 3 ppm. Values of $^1J(^{115}In,^{31}P)$ range from 550 ± 20 to 2500 ± 20 Hz. For any given halide, the $^1J(^{115}In,^{31}P)$ values generally increase with increasing basicity of the PR_3 ligand. Calculated values of $^1J(^{115}In,^{31}P)$ and $\Delta J(^{115}In,^{31}P)$ duplicate experimental trends and indicate that both the Fermi-contact and spin−dipolar Fermi-contact mechanisms make important contributions to the $^1J(^{115}In,^{31}P)$ tensors.

Introduction

Indium−phosphorus compounds have become important for numerous disciplines[1,2] including materials chemistry.[3−5] For example, semiconductors such as InP have attracted much attention because of their importance in applications such as light-emitting diodes.[1] The adducts formed by indium trihalide or indium trialkyl moieties with phosphine ligands, which are classical Lewis acid−base complexes, are single-source precursors for the preparation of a wide range of InP-based semiconductors.[4] The adducts of indium trihalides with triarylphosphine ligands, first prepared by Carty and Tuck over four decades ago,[6,7] possess either approximate tetrahedral $X_3In(PR_3)$ or trigonal−bipyramidal $X_3In(PR_3)_2$ (X = Cl, Br or I; PR_3 = triarylphosphine) structures (Chart 1),[8] depending on the bulkiness of both the halides and the triarylphosphine ligands.[8] Sterically demanding substituents generally lead to 1:1 adducts with approximately tetrahedral structures.

Chart 1

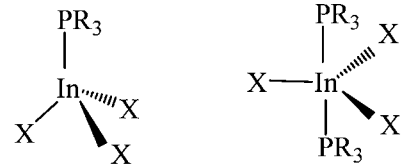

X = Cl, Br or I;

PR_3 = PPh_3, P(*o*-Anis)$_3$, P(*m*-Anis)$_3$, P(*p*-Anis)$_3$, TDP or TMP

Anis = anisole (methoxybenzene)
TDP = tris(2,6-dimethoxyphenyl)phosphine
TMP = tris(2,4,6-trimethoxyphenyl)phosphine

(1) (a) O'Brien, P.; Pickett, N. L. Coordination Complexes as Precursors for Semiconductor Films and Nanoparticles. In *Comprehensive Coordination Chemistry II*; McCleverty, J. A., Meyer, T. J., Eds.; Elsevier: Amsterdam, 2004; Vol. 9, Chapter 23, pp 1005−1063. (b) Grant, I. R. III-V Compounds. In *Chemistry of Aluminum, Gallium, Indium and Thallium*; Downs, A. J., Ed.; Blackie: London; 1993; Chapter 5, pp 292−321.

(2) (a) Trost, B. M.; Sharma, S.; Schmidt, T. *J. Am. Chem. Soc.* **1992**, *114*, 7903–7904. (b) Trost, B. M.; Sharma, S.; Schmidt, T. *Tetrahedron Lett.* **1993**, *34*, 7183–7186.

(3) van Weert, M. H. M.; Helman, A.; van den Einden, W.; Algra, R. E.; Verheijen, M. A.; Borgström, M. T.; Immink, G.; Kelly, J. J.; Kouwenhoven, L. P.; Bakkers, E. P. A. M. *J. Am. Chem. Soc.* **2009**, *131*, 4578–4579.

(4) (a) Wells, R. L.; Aubuchon, S. R.; Kher, S. S.; Lube, M. S. *Chem. Mater.* **1995**, *7*, 793–800. (b) Briand, G. G.; Davidson, R. J.; Decken, A. *Inorg. Chem.* **2005**, *44*, 9914–9920. (c) Malik, M. A.; O'Brien, P. *Top. Organomet. Chem.* **2005**, *9*, 173–204.

(5) (a) Tuck, D. G. Indium and Thallium. In *Comprehensive Coordination Chemistry*; Wilkinson, G., Gillard, R. D., McCleverty, J. A., Eds.; Pergamon: Oxford, 1987; Vol. 3, Chapter 25.2, pp 153−182. (b) Carty, A. J.; Tuck, D. G. *Prog. Inorg. Chem.* **1975**, *19*, 243–337.

(6) Carty, A. J.; Tuck, D. G. *J. Chem. Soc. A* **1966**, 1081–1087.

(7) Carty, A. J. *Can. J. Chem.* **1967**, *45*, 345–351.

(8) Rasika Dias, H. V. Indium and Thallium. In *Comprehensive Coordination Chemistry II*; McCleverty, J. A., Meyer, T. J., Eds.; Elsevier: Amsterdam, 2004; Vol. 3, pp 383−463.

Because there are spin-active isotopes of indium and phosphorus with high natural abundance, solid-state ^{115}In and ^{31}P NMR spectroscopy may provide insights into these adducts that are not readily available by other techniques. For example, the determination of indium and phosphorus chemical shift, CS, tensors, indirect spin−spin coupling constants between ^{115}In and ^{31}P nuclei, $^{1}J(^{115}\text{In},^{31}\text{P})$, and electric field gradient, EFG, tensors at indium can provide useful complementary structural information about the local indium and phosphorus environments. Solid-state indium NMR spectroscopy has traditionally been considered challenging because the two naturally occurring NMR-active isotopes, ^{113}In and ^{115}In, are quadrupolar nuclei ($S = 9/2$) with the largest nuclear quadrupole moments of the main group elements (^{113}In, N.A. = 4.28%, $Q = 75.9$ fm^2; ^{115}In, N.A. = 95.72%, $Q = 77.0$ fm^2).[9] The large Q values result in proportionally large nuclear quadrupolar coupling constants, which generally lead to broad NMR line shapes that are difficult to acquire experimentally. Despite its slightly larger nuclear quadrupole moment, ^{115}In is the preferred nucleus for NMR studies because of its much greater natural abundance.

Until recently, solid-state ^{115}In NMR studies have been mainly confined to compounds such as the indium spinel $CdIn_2S_4$[10] and the hexachloroindate anion, $InCl_6^{3-}$,[11] for which symmetry ensures that the EFGs at indium are small, resulting in nuclear quadruploar coupling constant values, $C_Q(^{115}\text{In})$, that are typically less than 50 MHz. Larger $C_Q(^{115}\text{In})$ values have been reported, but these were determined using either nuclear quadrupolar resonance (NQR)[12] or microwave spectroscopy.[13−15] However, indium CS and spin−spin coupling tensors cannot be characterized using NQR spectroscopy, and while high-resolution microwave spectroscopy can in principle provide such information,[16] the technique can only be applied to small molecules in the gas state, and thus only a few indium compounds, such as diatomic indium−halides,[13,17,18] InOH,[14] and $In(C_5H_5)$[15] have been studied by this technique. Recent work in our lab has demonstrated that obtaining ^{115}In NMR spectra of solid samples with $C_Q(^{115}\text{In})$ values as large as 250−300 MHz is feasible.[19] Broad central-transition powder patterns for ^{115}In NMR spectra were acquired with either the quadrupolar-echo[20] or the quadrupolar Carr−Purcell Meiboom−Gill (QCPMG)[21,22] pulse sequences, in conjunction with the stepped-frequency technique.[23−25] From the known range of isotropic indium chemical shift values, $\delta_{iso}(\text{In})$, ~1100 ppm,[26] one might expect the orientation dependence of the chemical shifts to be significant, but such information for solid indium compounds has not been systematically investigated.

In this contribution, a series of triarylphosphine indium trihalide adducts, $X_3In(PR_3)$ and $X_3In(PR_3)_2$ (Chart 1) are investigated by determining and interpreting their indium EFG and CS tensors; these results are corroborated by the results of density functional theory (DFT) calculations. Possible causes for the observed sensitivity of the indium CS tensors to the nature of the halogen ligands are considered. In addition, analysis of the ^{31}P NMR spectra allowed the determination of $^{1}J(^{115}\text{In},^{31}\text{P})$ values, and for several of these adducts, $\Delta J(^{115}\text{In},^{31}\text{P})$, the anisotropy in $^{1}J(^{115}\text{In},^{31}\text{P})$, was also determined. Previously, $\Delta J(^{115}\text{In},^{31}\text{P})$ has only been determined from an analysis of the ^{31}P NMR spectra of $Br_3In[P(p\text{-Anis})_3]$.[27] The signs for $\Delta J(^{115}\text{In},^{31}\text{P})$, $^{1}J(^{115}\text{In},^{31}\text{P})$, and $C_Q(^{115}\text{In})$ were also determined for high-symmetry adducts. Finally, since knowledge of the structures of the adducts under study is invaluable for a proper analysis of the ^{115}In and ^{31}P NMR spectra, single-crystal X-ray diffraction data for several of these compounds are also presented.

Theory and Background

Indium NMR Spectroscopy. The ^{115}In nuclei for the complexes considered here are subject to the Zeeman, nuclear quadrupolar, and nuclear magnetic shielding interactions, and since they are directly bonded to one or two ^{31}P nuclei ($I = 1/2$, NA = 100%), they are also subject to the direct dipolar and indirect nuclear spin−spin coupling interactions.

The nuclear quadrupolar coupling describes the interaction of the nuclear quadrupole moment, eQ, with the EFG at the nucleus;[28] the latter is described by a symmetric traceless second-rank tensor which, when in its principal axis system (PAS), is diagonal and may be characterized by two independent parameters: $C_Q = eQV_{ZZ}/h$ (in Hz), where $|V_{ZZ}| = |eq_{ZZ}|$ is the principal component of the EFG tensor with the greatest magnitude, and the asymmetry parameter, $\eta_Q = (V_{XX} - V_{YY})/V_{ZZ}$ with $0 \le \eta_Q \le 1$ and $|V_{XX}| \le |V_{YY}| \le |V_{ZZ}|$. For the systems considered here, the quadrupolar interaction can be treated as a perturbation of the Zeeman interaction (*vide infra*); therefore, it is convenient to discuss the results of both first- and second-order perturbation theory.[28,29] To first order, the quadrupolar interaction has no effect on the central transition, $m_s = 1/2 \rightarrow m_s = -1/2$, but defines the line shape of the satellite transitions.[28] However, to second order, the quadrupolar interaction affects all allowed NMR transitions (nine for $S = 9/2$ nuclei).[28]

(9) Pyykkö, P. *Mol. Phys.* **2008**, *106*, 1965–1974.
(10) Breuer, A.; Siebert, D. *Ber. Bunsen Ges. Phys. Chem.* **1996**, *100*, 1736–1739.
(11) Yamada, K.; Kumano, K.; Okuda, T. *Solid State Ionics* **2005**, *176*, 823–829.
(12) Bastow, T. J.; West, G. W. *J. Phys.: Condens. Matter* **2003**, *15*, 8389–8406.
(13) Hensel, K. D.; Gerry, M. C. L. *J. Chem. Soc., Faraday Trans.* **1997**, *93*, 1053–1059.
(14) Lakin, N. M.; Varberg, T. D.; Brown, J. M. *J. Mol. Spectrosc.* **1997**, *183*, 34–41.
(15) Drouin, B. J.; Cassak, P. A.; Briggs, P. M.; Kukolich, S. G. *J. Chem. Phys.* **1997**, *107*, 3766–3773.
(16) Bryce, D. L.; Wasylishen, R. E. *Acc. Chem. Res.* **2003**, *36*, 327–334.
(17) Barrett, A. H.; Mandel, M. *Phys. Rev.* **1958**, *109*, 1572–1589.
(18) Walker, N. R.; Francis, S. G.; Rowlands, J. J.; Legon, A. C. *J. Mol. Spectrosc.* **2006**, *239*, 126–129.
(19) Chen, F.; Ma, G.; Cavell, R. G.; Terskikh, V. V.; Wasylishen, R. E. *Chem. Commun.* **2008**, 5933–5935.
(20) Bodart, P. R.; Amoureux, J.-P.; Dumazy, Y.; Lefort, R. *Mol. Phys.* **2000**, *98*, 1545–1551.
(21) Larsen, F. H.; Jakobsen, H. J.; Ellis, P. D.; Nielsen, N. C. *J. Phys. Chem. A* **1997**, *101*, 8597–8606.
(22) Lipton, A. S.; Heck, R. W.; Ellis, P. D. *J. Am. Chem. Soc.* **2004**, *126*, 4735–4739.
(23) (a) Kennedy, M. A.; Vold, R. L.; Vold, R. R. *J. Magn. Reson.* **1991**, *92*, 320–331. (b) Bastow, T. J.; Smith, M. E.; Stuart, S. N. *Chem. Phys. Lett.* **1992**, *191*, 125–129.
(24) Ooms, K. J.; Bernard, G. M.; Kadziola, A.; Kofod, P.; Wasylishen, R. E. *Phys. Chem. Chem. Phys.* **2009**, *11*, 2690–2699.
(25) (a) Lipton, A. S.; Wright, T. A.; Bowman, M. K.; Reger, D. L.; Ellis, P. D. *J. Am. Chem. Soc.* **2002**, *124*, 5850–5860. (b) Bryant, P. L.; Butler, L. G.; Reyes, A. P.; Kuhns, P. *Solid State Nucl. Magn. Reson.* **2000**, *16*, 63–67.
(26) Akitt, J. W. Aluminum, Gallium, Indium and Thallium. In *Multinuclear NMR*; Mason, J., Ed.; Plenum Press: New York, 1987; Chapter 9, pp 259−292.
(27) Wasylishen, R. E.; Wright, K. C.; Eichele, K.; Cameron, T. S. *Inorg. Chem.* **1994**, *33*, 407–408.
(28) Abragam, A. *Principles of Nuclear Magnetism*; Clarendon Press: Oxford, 1961; Chapter VII, pp 216−263.
(29) Bain, A. D. *J. Magn. Reson.* **2006**, *179*, 308–310.

It should be noted that the third-order perturbation term does not contribute to the line shape of the central transition for half-integer quadrupolar nuclei.[29] In the absence of anisotropic magnetic shielding, the maximum and minimum frequencies of the central transition for $S = 9/2$ nuclei of a stationary sample with axial symmetry are $\nu_S + C_Q^2/(384\nu_S)$ and $\nu_S - C_Q^2/(216\nu_S)$, respectively,[30] where ν_S is the isotropic resonance frequency for the quadrupolar nucleus S. From the inverse dependence of these expressions on ν_S (and hence of the breadth of the NMR powder pattern), it is apparent that obtaining NMR spectra of the central transition at the highest practical applied magnetic field strength is usually advantageous, particularly for nuclei with large values of C_Q.

In the nonrelativistic theory proposed by Ramsey,[31] nuclear magnetic shielding is expressed as the sum of diamagnetic, σ_{dia}, and paramagnetic, σ_{para}, terms. For heavy atoms, spin−orbit effects on the shielding are substantial, and thus this factor, $\sigma_{spin-orbit}$, is often included in discussions of their nuclear magnetic shielding.[32] This effect is now accepted to be the source of the long-known relativistic effect on nuclear magnetic shielding.[33,34]

The magnetic shielding experienced by a nucleus is affected by the local environment experienced by that nucleus and thus is generally dependent on the orientation of the molecule relative to $\mathbf{B}_0$. The shielding is described by a second-rank tensor, $\boldsymbol{\sigma}$, which is diagonal in its PAS with three principal components, σ_{11}, σ_{22}, and σ_{33}, where $\sigma_{11} \leq \sigma_{22} \leq \sigma_{33}$.[35] In practice, NMR spectroscopists measure chemical shifts, δ, the nuclear magnetic shielding of a given nucleus relative to that for a reference compound. The chemical shift is related to the magnetic shielding by $\delta_{sample} \approx \sigma_{ref} - \sigma_{sample}$, where the latter two terms refer to the magnetic shielding of the reference compound and of the sample, respectively.[35] When discussing NMR spectra, it is convenient to use three magnetic shielding or chemical shift parameters: the isotropic nuclear magnetic shielding, $\sigma_{iso} = (1/3)\mathrm{Tr}(\boldsymbol{\sigma})$, or the isotropic chemical shift, $\delta_{iso} = (\delta_{11} + \delta_{22} + \delta_{33})/3$, where $\delta_{11} \geq \delta_{22} \geq \delta_{33}$, the span, $\Omega = \sigma_{33} - \sigma_{11} = \delta_{11} - \delta_{33}$, describing the maximum orientation dependence of the magnetic shielding interaction, and the skew, $\kappa = 3(\sigma_{iso} - \sigma_{22})/\Omega = 3(\delta_{22} - \delta_{iso})/\Omega$, which is unitless with $-1 \leq \kappa \leq +1$.[35]

The isotropic indirect spin−spin coupling constant, J, between I and S is given by $(1/3)\mathrm{Tr}(\mathbf{J})$,[36,37] where $\mathbf{J}$ is the indirect spin−spin coupling tensor. When the two coupled nuclei lie on a C_n symmetry axis with $n \geq 3$, $\mathbf{J}$ is axially symmetric with the unique component coincident with the dipolar vector, r_{IS}; in such cases, the anisotropy of $\mathbf{J}$, ΔJ, is $J_{\parallel} - J_{\perp}$.[36,37] The dipolar interaction describes the through-space interaction between two spins, I and S. The magnitude of this interaction is represented by the dipolar coupling constant:

$$R_{DD} = \left(\frac{\mu_0}{4\pi}\right)\frac{\gamma_I\gamma_S\hbar}{2\pi}\langle r_{IS}^{-3}\rangle \qquad (1)$$

where r_{IS} is the internuclear separation.[37] Experimentally, one measures an effective dipolar coupling constant, R_{eff}. Recalling that we are considering the case where the dipolar and $\mathbf{J}$ tensors are conincident, $R_{eff} = R_{DD} - \Delta J/3$.[37] If r_{IS} is known, R_{DD} can be calculated from eq 1 and if R_{eff} is determined from NMR experiments, the magnitude of ΔJ may be estimated.

Phosphorus-31 NMR Spectroscopy of the ^{115}In−^{31}P Spin Pair. If under MAS conditions the breadth of the central transition of an ^{115}In NMR spectrum exceeds the maximum practical spinning frequency, one must obtain and analyze spectra of stationary samples. This does not preclude the determination of ^{115}In NMR parameters (*vide infra*), but the methods may be time-consuming. As an alternative, or to corroborate data obtained by ^{115}In NMR spectroscopy, one may determine some ^{115}In quadrupolar parameters indirectly if the ^{115}In nuclei are spin−spin coupled to a spin-1/2 nucleus, such as ^{31}P for the samples considered here.[38]

In the high-field approximation (only valid if the ratio $C_Q/[4S(2S-1)\nu_S]$ is small) the isotropic region of an NMR spectrum of a ^{31}P nucleus spin−spin coupled to ^{115}In consists of 10 peaks split by $J(^{115}\mathrm{In},^{31}\mathrm{P})$ (Figure 1, upper trace).[38] However, if this ratio is significant, the direct dipolar interaction for the ^{115}In−^{31}P spin pair is not averaged to zero by magic angle spinning (MAS),[38] a consequence of the fact that the indium nuclei are not quantized exactly along $\mathbf{B}_0$.[39] In this case, one observes an uneven spacing between the peaks in the ^{31}P NMR spectra, described by:[40]

$$\nu_m = \nu_L - m_s|J_{iso}| + \frac{[S(S+1) - 3m^2]}{S(2S-1)}d \qquad (2)$$

where m_s is the quantum spin-state of the ^{115}In nucleus, ν_L is the isotropic NMR frequency of the ^{31}P nucleus, and d is the residual dipolar coupling constant, defined as

$$d = +\frac{3C_QR_{eff}}{20\nu_S}[(3\cos^2\beta^D - 1) + \eta_Q\sin^2\beta^D\cos 2\alpha^D] \qquad (3)$$

Here, β^D and α^D are polar angles describing the orientation of the ^{115}In−^{31}P dipolar vector with respect to the principal components of the EFG tensor at the ^{115}In nucleus. It should be noted that in eq 3 the $\mathbf{J}$ and dipolar tensors are assumed to be

(30) Amoureux, J. P.; Fernandez, C.; Granger, P. Interpretation of Quadrupolar Powder Spectra: Static and MAS Experiments. In *Multinuclear Magnetic Resonance in Liquids and Solids - Chemical Applications*; Granger, P. Harris, R. K., Eds.; NATO ASI Series C: Mathematical and Physical Sciences; Kluwer Academic Publishers: Dordrecht; 1990, pp 409−424.
(31) Ramsey, N. F. *Phys. Rev.* **1950**, *78*, 699–703.
(32) Pyykkö, P.; Görling, A.; Rösch, N. *Mol. Phys.* **1987**, *61*, 195–205.
(33) (a) Sugimoto, M.; Kanayama, M.; Nakatsuji, H. *J. Phys. Chem.* **1993**, *97*, 5868–5874. (b) Takashima, H.; Hada, M.; Nakatsuji, H. *Chem. Phys. Lett.* **1995**, *235*, 13–16.
(34) Autschbach, J.; Ziegler, T. Relativistic Computation of NMR Shieldings and Spin-Spin Coupling Constants. In *Encyclopedia of Nuclear Magnetic Resonance*; Grant, D. M., Harris, R. K., Eds.; John Wiley & Sons: Chichester, 2002; Vol. 9, pp 306−323.
(35) Mason, J. *Solid State Nucl. Magn. Reson.* **1993**, *2*, 285–288.
(36) Buckingham, A. D.; Love, I. *J. Magn. Reson.* **1970**, *2*, 338–351.
(37) (a) Wasylishen, R. E. Dipolar and Indirect Coupling Tensors in Solids. In *Encyclopedia of Nuclear Magnetic Resonance*; Grant, D. M., Harris, R. K., Eds.; John Wiley & Sons: Chichester, 1996; Vol. 3, pp 1685−1695. (b) Wasylishen, R. E. Indirect Nuclear Spin-Spin Coupling Tensors. In *Encyclopedia of Nuclear Magnetic Resonance*; Grant, D. M., Harris, R. K., Eds.; John Wiley & Sons: Chichester, 2002; Vol. 9, pp 274−282 and references cited therein.
(38) (a) Harris, R. K.; Olivieri, A. C. *Prog. Nucl. Magn. Reson. Spectrosc.* **1992**, *24*, 435–456, and references cited therein. (b) Harris, R. K.; Olivieri, A. C. Spinning Sideband Analysis for Spin-1/2 Nuclei. In *Encyclopedia of Nuclear Magnetic Resonance*; Grant, D. M., Harris, R. K., Eds.; John Wiley & Sons: Chichester, 2002; Vol. 9, pp 141−150. (c) Grondona, P.; Olivieri, A. C. *Concepts Magn. Reson.* **1993**, *5*, 319–339.
(39) VanderHart, D. L.; Gutowsky, H. S.; Farrar, T. C. *J. Am. Chem. Soc.* **1967**, *89*, 5056–5057.
(40) (a) Olivieri, A. C. *Solid State Nucl. Magn. Reson.* **1992**, *1*, 345–353. (b) Olivieri, A. C. *J. Magn. Reson.* **1989**, *81*, 201–205.

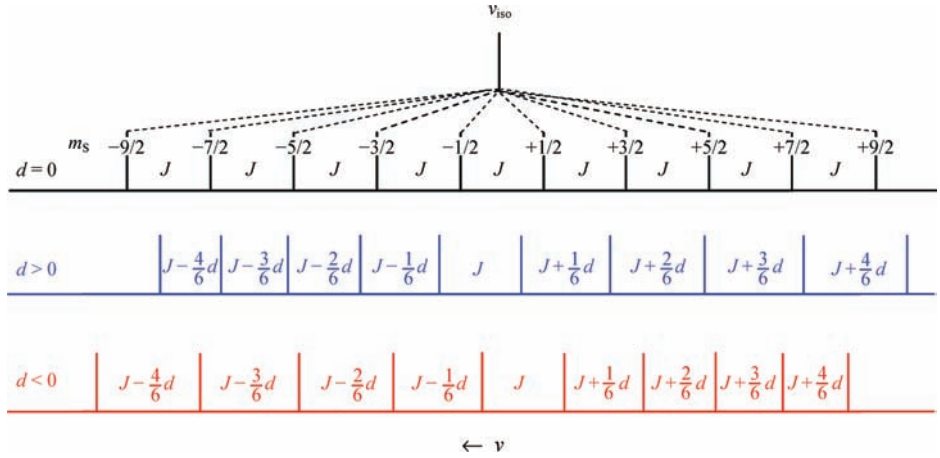

Figure 1. Calculated splitting pattern in a ^{31}P NMR spectrum of an MAS sample containing an ^{115}In−^{31}P spin pair with $d = 0$, $d > 0$, and $d < 0$ (see eq 3 for the definition of d). The spin states as indicated are those for a positive sign for $^{1}J(^{115}\text{In},^{31}\text{P})$, but the splitting pattern is invariant to this sign.

coincident; more general equations are available in the literature.[40] If J_{iso} and R_{eff} make detectable contributions to the ^{31}P NMR spectra, β^D and α^D may be determined from those of MAS and stationary samples. As shown in Figure 1, in the presence of significant residual dipolar coupling, the d value can be obtained experimentally, from which one may obtain information about C_Q (eq 3). If $|C_Q|$ is determined from other experiments (*e.g.*, ^{115}In NMR experiments for the samples considered here) and if the values for β^D and α^D may be surmised from molecular symmetry, the sign for C_Q may be determined from the "sense" of the spectrum (i.e., whether the splitting between peaks increases or decreases with increasing frequency). Since simulations of NMR spectra of quadrupolar nuclei are invariant to the sign of C_Q, this is the only NMR technique that allows the determination of the sign of C_Q. For several of the samples considered here, d was of sufficient magnitude to allow the determination of the sign of C_Q or to corroborate the value for $C_Q(^{115}\text{In})$ determined from ^{115}In NMR. Note that d describes the center of mass for the individual peaks of the multiplets. In principle, each of these peaks has a distinct line shape,[38] but as shown below, the line shapes are not detectable for the ^{31}P NMR spectra considered here.

Experimental and Computational Details

Sample Preparation. $InCl_3$, $InBr_3$, InI_3, and tris(*p*-methoxyphenyl)phosphine, P(*p*-Anis)$_3$; tris(*m*-methoxyphenyl)phosphine, P(*m*-Anis)$_3$; and tris(2,4,6-trimethoxyphenyl)phosphine, TMP, were purchased from Strem Chemicals. Triphenylphosphine, PPh_3; tris(2,6-dimethoxyphenyl)phosphine, TDP; and tris(*o*-methoxyphenyl)phosphine, P(*o*-Anis)$_3$, were purchased from Alfa Aesar. All commercial compounds were used as received. Owing to the ease of hydrolysis of the anhydrous indium halides and oxidation of the phosphine ligands, all syntheses were carried out in a dry glovebox under argon. Anhydrous solvents were used in all the preparations.

Similar procedures were used for the synthesis of all the triarylphosphine indium trihalide adducts. Unless otherwise noted, reactions were carried out in ethyl acetate. All adducts were prepared by adding a solution of the anhydrous indium(III) trihalide, dissolved in selected organic solvents, to a stoichiometric amount of the phosphine ligands in the same solvent. During stirring, white or light-green powders of these adducts precipitated and were filtered, washed with a small amount of the same solvent, and dried in vacuo. Elemental analysis (EA) was carried out for all adducts synthesized here: $Br_3In(TMP)$, $I_3In(TMP)$, $Cl_3In(TDP)$, $Br_3In(TDP)$, $I_3In(TDP)$, $Cl_3In[P(o\text{-Anis})_3]\cdot P(o\text{-Anis})_3$, $Cl_3In[P(o\text{-Anis})_3]$, $Br_3In[P(o\text{-Anis})_3]$, $I_3In[P(o\text{-Anis})_3]$, $Cl_3In[P(m\text{-Anis})_3]_2$, $Br_3In[P(m\text{-Anis})_3]$, $\{I_3In[P(m\text{-Anis})_3]\}_{0.97}\cdot\{I_3In[P(m\text{-Anis})_3]_2\}_{0.03}$, and $\{I_3In[P(m\text{-Anis})_3]\}_{0.19}\cdot\{I_3In[P(m\text{-Anis})_3]_2\}_{0.81}$; see Supporting Information for a summary of these results. The preparation of $Cl_3In(TMP)$ was reported in our earlier communication.[19] $Cl_3In[P(p\text{-Anis})_3]_2$,[7] $Br_3In[P(p\text{-Anis})_3]$,[7,27] $I_3In[P(p\text{-Anis})_3]_2$,[7] $Cl_3In(PPh_3)_2$,[41] $Br_3In(PPh_3)_2$,[6] $I_3In(PPh_3)$ (reaction in cyclohexane),[42] and $I_3In(PPh_3)_2\cdot I_3In(PPh_3)$ (reaction in ethyl acetate)[42,43] were prepared according to literature methods. The preparations were carried out under an inert atmosphere, but all synthesized adducts are stable in air for moderate periods of time.

Single-Crystal X-ray Diffraction. Single crystals were grown by very slow evaporation of the solvents. Suitable crystals were mounted on glass fibers by means of paratone-N oil, and data were collected at 193 K using graphite-monochromated Mo Kα radiation (0.71073 Å) on a Bruker PLATFORM/SMART 1000 CCD diffractometer. The structures were solved by Patterson search/structure expansion (*DIRDIF-99*)[44] or by direct methods (*SHELXS-97*)[45] and refined using full-matrix least-squares on F^2 (*SHELXL-97*).[45] All non-hydrogen atoms in the structure were refined with anisotropic displacement parameters. Selected crystal data and structure refinement details for the triarylphosphine indium trihalide adducts are available from Supporting Information.

Solid-State NMR Spectroscopy. Samples were packed in 4 mm o.d. rotors. Phosphorus-31 NMR spectra were acquired using a Chemagnetics CMX Infinity 200 ($B_0 = 4.70$ T) as well as Bruker Avance 300 ($B_0 = 7.05$ T) and 500 ($B_0 = 11.75$ T) NMR spectrometers using the combination of cross-polarization (CP), ^{1}H two-pulse phase modulation (TPPM) decoupling[46] and magic angle spinning (MAS). Proton 90° pulse widths of 2.5 or 4.0 μs, contact times of 5−10 ms and recycle delays of 4− 8 s were used to acquire most ^{31}P NMR spectra. Phosphorus-31 chemical shifts were referenced with respect to 85% aqueous phosphoric acid ($\delta_{iso} = 0$) by setting the isotropic peak of an external solid ammonium dihydrogen phosphate sample to 0.8 ppm.[47] All spectra were acquired at ambient temperature with a spinning frequency ranging from 8.0 to 15.0 kHz.

(41) Veidis, M. V.; Palenik, G. J. *J. Chem. Soc. D* **1969**, 586–587.
(42) Brown, M. A.; Tuck, D. G.; Wells, E. J. *Can. J. Chem.* **1996**, *74*, 1535–1549.
(43) Godfrey, S. M.; Kelly, K. J.; Kramkowski, P.; McAuliffe, C. A.; Pritchard, R. G. *Chem. Commun.* **1997**, 1001–1002.
(44) Beurskens, P. T.; Beurskens, G.; de Gelder, R.; Garcia-Granda, S.; Israel, R.; Gould, R. O.; Smits, J. M. M. *The DIRDIF-99 Program System*; Crystallography Laboratory, University of Nijmegen: Nijmegen, the Netherlands, 1999.
(45) Sheldrick, G. M. *Acta Crystallogr.* **2008**, *A64*, 112–122.
(46) Bennett, A. E.; Rienstra, C. M.; Auger, M.; Lakshmi, K. V.; Griffin, R. G. *J. Chem. Phys.* **1995**, *103*, 6951–6958.
(47) Eichele, K.; Wasylishen, R. E. *J. Phys. Chem.* **1994**, *98*, 3108–3113.

Indium-115 NMR spectra of stationary samples were acquired using either quadrupolar-echo[20] or QCPMG[21] pulse sequences; where necessary (typically, spectra whose breadth exceeded 100 kHz), the stepped-frequency technique[23] was used. Bruker Avance 300 and 500 NMR spectrometers, with ^{115}In NMR frequencies of 65.8 and 109.6 MHz, respectively, and a Bruker Avance II 900 NMR spectrometer (21.14 T), with a ^{115}In NMR frequency of 197.2 MHz, were used to acquire all spectra. A relaxation delay of 0.5 s was used for all samples. For the solid-state NMR experiments, the ^{115}In 90° pulse widths, $\tau_{(sel)}$, that selectively excited the central transition were set as $\tau_{(sel)} = \tau_{(nonsel)}/(S + 1/2) = \tau_{(nonsel)}/5$.[20] The $\tau_{(sel)}$ value was 0.4 μs for spectra acquired at 7.05 and 11.75 T, and 0.5 μs for spectra acquired at 21.14 T. Proton decoupling was achieved using the TPPM scheme.[46] Each step of the ^{115}In NMR spectra acquired at 7.05 or 11.75 T is the sum of 29020 to 77824 scans. Experimental conditions for the QCPMG pulse sequence were set following literature procedures,[21] with 1024 or 2048 scans for each step. The individual stepped-frequency spectra were coadded using the skyline projection method.[48] In-115 NMR chemical shifts were referenced with respect to an external solution of 0.1 M $In(NO_3)_3$ in 0.5 M HNO_3 ($\delta_{iso} = 0$). Phosphorus-31 and indium-115 NMR parameters were determined by visual comparison of experimental NMR spectra with those simulated using the WSolids software package.[49] This software includes the quadrupolar interaction to second-order perturbation theory for simulations of ^{115}In NMR spectra, and includes spin−spin interactions with ^{115}In for simulations of ^{31}P NMR spectra of MAS samples.

Quantum Chemical Calculations. DFT calculations of indium CS[50] and EFG tensors,[51] as well as the $^1J(^{115}In,^{31}P)$ and $\Delta J(^{115}In,^{31}P)$ values,[52] were performed using the Amsterdam Density Functional (ADF) program.[53] The Vosko−Wilk−Nusair (VWN) local density approximation,[54] with the Becke−Perdew generalized gradient approximation (GGA),[55] was used for the exchange-correlation functional. All calculations allowed for relativistic effects, including spin−orbital and scalar corrections, and were carried out using the zeroth-order regular approximation (ZORA) formalism.[56] The ^{115}In EFG values determined using this software are based on a value for Q of 81.0 fm^2, rather than the more recent value summarized by Pyykkö;[9] calculated values reported here have been scaled by a factor of 0.951 to incorporate the more recent value for $Q(^{115}In)$. The Fermi-contact (FC), spin dipolar (SD), paramagnetic spin−orbital (PSO) and diamagnetic spin−orbital (DSO) mechanisms were included in all J calculations;[36,57] a description of these mechanisms, as implemented in the ZORA formalism, has been presented.[52] ADF uses Slater-type basis sets; for the results presented herein, the QZ4P basis set, which is of quadruple-ζ quality with four sets of polarization functions and is optimized for ZORA calculations, was used for indium, phosphorus, oxygen, chlorine, bromine and iodine atoms and the TZP basis set, of triple-ζ quality with one set of polarization functions, also optimized for ZORA calculations, was used for the H and C atoms.

Geometries of the $X_3In(PR_3)_n$ ($n = 1$ or 2) adducts obtained from X-ray diffraction were used for the calculations. To reduce computational time, the PR_3 ligands in the trigonal−bipyramidal $X_3In(PR_3)_2$ adducts were replaced by PMe_3 ligands without changing the geometry of the X_3InP_2 core. To investigate the effects of the halides and of the geometry on the indium magnetic shielding, CS tensors for model $X_3In(PMe_3)$ and $X_3In(PMe_3)_2$ (X = Cl, Br, or I) adducts with a C_3 symmetry axis were also calculated. The apparent correlation between $^1J(^{115}In,^{31}P)$ and the basicity of the triarylphosphine ligands was investigated by calculating the $^1J(^{115}In,^{31}P)$ and $\Delta J(^{115}In,^{31}P)$ values as well as their signs for $Cl_3In(PR_3)$ and $Br_3In(PR_3)$ adducts. The geometries used for the latter were those obtained from X-ray crystallography, where available. If such data were unavailable, the structures for $Cl_3In(TMP)$ or $Br_3In(TMP)$ were used, with the methoxy groups replaced by H where needed (e.g., the para methoxy groups of TMP were replaced with hydrogen atoms to model the TDP ligand). Because of the long computational time, it was impractical to undertake DFT calculations of $^1J(^{115}In,^{31}P)$ and $\Delta J(^{115}In,^{31}P)$ for $I_3In(PR_3)$ or for the trigonal−bipyramidal adducts.

Results and Discussion

This section is organized as follows: first, the molecular structures of the triarylphosphine indium trihalide adducts are discussed. Next, solid-state ^{115}In NMR spectra for each adduct are presented and interpreted. Third, the $^1J(^{115}In,^{31}P)$ values for all complexes, determined *via* ^{31}P NMR spectroscopy, are considered. For complexes with an exact or approximate C_3 axis, the $\Delta J(^{115}In,^{31}P)$ values and the signs for $\Delta J(^{115}In,^{31}P)$ and $C_Q(^{115}In)$ are also presented. Finally, relativistic DFT calculations of NMR parameters for these compounds are compared with the experimental values and the causes of the observed sensitivity of the indium CS tensors to the nature of the directly bonded halogen ligands are explored.

Structures of the Triarylphosphine Indium Trihalide Adducts. Structural data obtained *via* X-ray crystallography are important for this study, to relate NMR data with structure. Single-crystal structures for $Cl_3In(PPh_3)_2$,[41] $I_3In(PPh_3)$,[42] $I_3In(PPh_3)_2 \cdot I_3In(PPh_3)$,[42] $Cl_3In(TMP)$,[19] and $Br_3In[P(p\text{-Anis})_3]$[27] have been reported previously. The structures for nine additional adducts were determined as part of this study; see Tables S1 and S2 in Supporting Information for more detailed X-ray diffraction data and for selected structural information.

We were unable to obtain crystals suitable for X-ray diffraction studies for adducts containing the $P(m\text{-Anis})_3$ or TDP ligands. However, EA combined with solid-state ^{31}P NMR (*vide infra*) established whether 1:1 or 2:1 adducts were formed and confirmed the In−P connectivity. Existing structural data[8] as well as that presented here have shown that 1:1 and 2:1 triarylphosphine indium(III) trihalide adducts adopt approximate tetrahedral or trigonal−bipyramidal geometries about the indium atom, respectively. In the ensuing discussion, adducts are assumed to adopt one of these two structures, depending on the EA and NMR data, if X-ray diffraction data are unavailable.

Adducts formed by $InCl_3$ with less crowded phosphine ligands adopt 2:1 trigonal−bipyramidal structures: $Cl_3In[P(p\text{-Anis})_3]_2$,[7] $Cl_3In[P(m\text{-Anis})_3]_2$, and $Cl_3In(PPh_3)_2$;[41] in contrast, crowded phosphine ligands such as TMP or TDP form 1:1 adducts which have approximately tetrahedral structures. See Figures 2a and 2b for examples of tetrahedral and trigonal−bipyramidal

(48) (a) Nagayama, K.; Bachmann, P.; Wüthrich, K.; Ernst, R. R. *J. Magn. Reson.* **1978**, *31*, 133–148. (b) Blümich, B.; Ziessow, D. *J. Magn. Reson.* **1982**, *49*, 151–154.
(49) Eichele, K.; Wasylishen, R. E. *WSOLIDS*, Version 2.0.18; University of Alberta: Edmonton, Canada, 2000.
(50) Schreckenbach, G.; Ziegler, T. *J. Phys. Chem.* **1995**, *99*, 606–611.
(51) van Lenthe, E.; Baerends, E. J. *J. Chem. Phys.* **2000**, *112*, 8279–8292.
(52) (a) Autschbach, J.; Ziegler, T. *J. Chem. Phys.* **2000**, *113*, 9410–9418. (b) Autschbach, J.; Ziegler, T. *J. Chem. Phys.* **2000**, *113*, 936–947.
(53) (a) *ADF*, 2006.01; Theoretical Chemistry, Vrije Universiteit: Amsterdam, 2006; http://www.scm.com. (b) te Velde, G.; Bickelhaupt, F. M.; Baerends, E. J.; Fonseca Guerra, C.; van Gisbergen, S. J. A.; Snijders, J. G.; Zeigler, T. *J. Comput. Chem.* **2001**, *22*, 931–967. (c) Fonseca Guerra, C.; Snijders, J. G.; te Velde, G.; Baerends, E. J. *Theor. Chem. Acc.* **1998**, *99*, 391–403.
(54) Vosko, S. H.; Wilk, L.; Nusair, M. *Can. J. Phys.* **1980**, *58*, 1200–1211.
(55) (a) Becke, A. D. *Phys. Rev. A* **1988**, *38*, 3098–3100. (b) Perdew, J. P. *Phys. Rev. B* **1986**, *33*, 8822–8824. (c) Perdew, J. P. *Phys. Rev. B* **1986**, *34*, 7406.
(56) (a) van Lenthe, E.; Baerends, E. J.; Snijders, J. G. *J. Chem. Phys.* **1993**, *99*, 4597–4610. (b) van Lenthe, E.; Baerends, E. J.; Snijders, J. G. *J. Chem. Phys.* **1994**, *101*, 9783–9792. (c) van Lenthe, E.; Ehlers, A.; Baerends, E. J. *J. Chem. Phys.* **1999**, *110*, 8943–8953.
(57) Vaara, J.; Jokisaari, J.; Wasylishen, R. E.; Bryce, D. L. *Prog. Nucl. Magn. Reson. Spectrosc.* **2002**, *41*, 233–304.

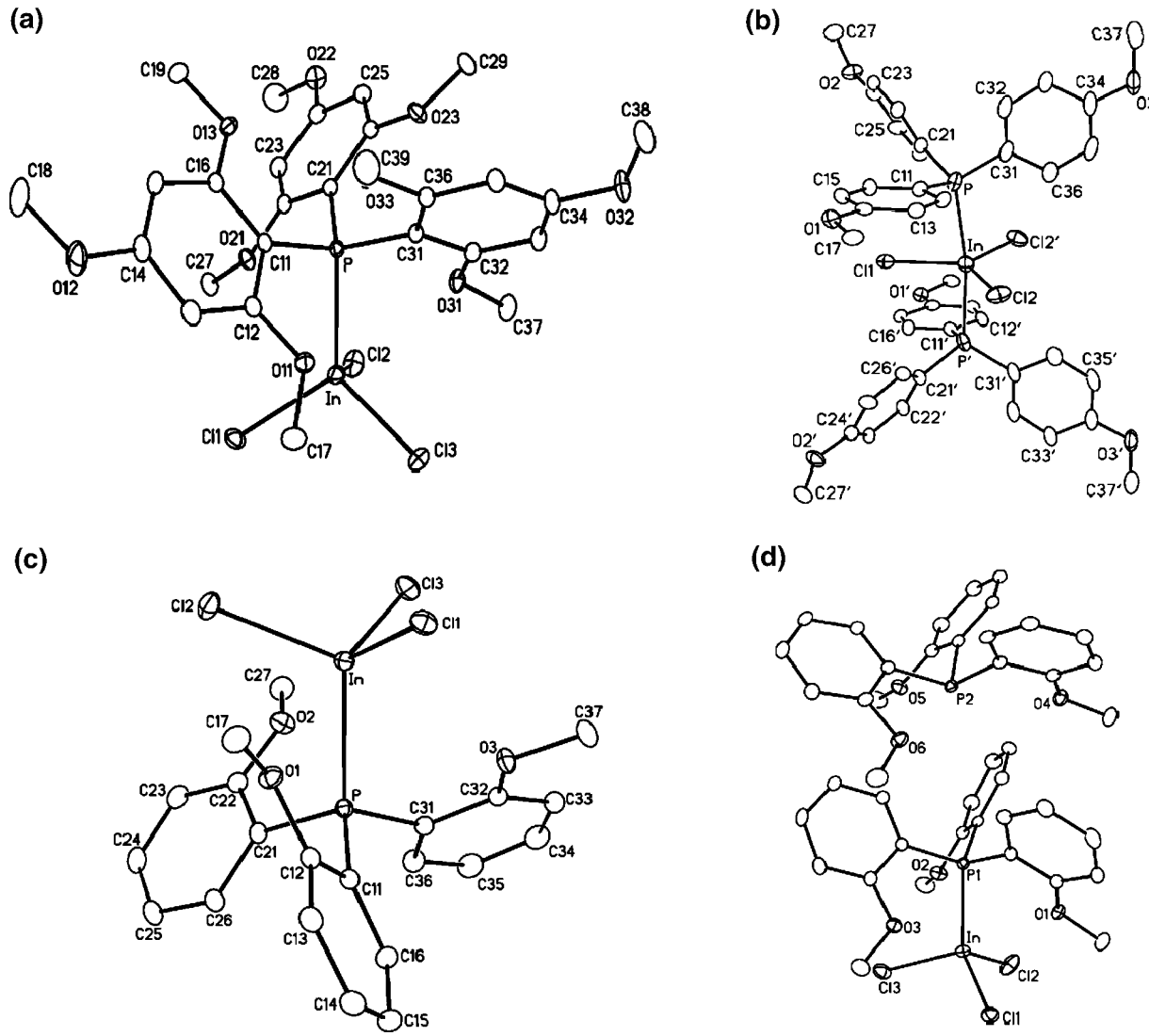

Figure 2. Molecular structures of (a) $Cl_3In(TMP)$,[19] (b) $Cl_3In[P(p\text{-Anis})_3]_2$, (c) $Cl_3In[P(o\text{-Anis})_3]$ and (d) $Cl_3In[P(o\text{-Anis})_3]\cdot P(o\text{-Anis})_3$.

structures, respectively. EA results indicate that the adducts of $InCl_3$ with $P(o\text{-Anis})_3$ can adopt either the 1:1 or 2:1 structures, depending on the ratio of $InCl_3$ to $P(o\text{-Anis})_3$ used in the synthesis; the former adopts a tetrahedral structure (Figure 2c). Surprisingly, single-crystal X-ray diffraction data indicate that the 2:1 adduct does not have a trigonal−bipyramidal structure, but instead forms tetrahedral $Cl_3In[P(o\text{-Anis})_3]$ with an additional uncoordinated $P(o\text{-Anis})_3$ molecule packed in the same unit cell (Figure 2(d)); thus, the molecular formula is $Cl_3In[P(o\text{-Anis})_3]\cdot P(o\text{-Anis})_3$.

For the $InBr_3$ adducts considered here, only $Br_3In(PPh_3)_2$ adopts the trigonal−bipyramidal structure; the remaining adducts, $Br_3In[P(o\text{-Anis})_3]$, $Br_3In[P(p\text{-Anis})_3]$,[27] $Br_3In[P(m\text{-Anis})_3]$, $Br_3In(TDP)$, and $Br_3In(TMP)$, are tetrahedral, presumably due to the bulkiness of the Br atoms.

Adducts formed by InI_3 with $P(o\text{-Anis})_3$, $P(p\text{-Anis})_3$, TDP, and TMP are approximately tetrahedral; the structures of the InI_3 adducts with PPh_3 or $P(m\text{-Anis})_3$ depend on the solvents used for the synthesis. Those with PPh_3 can crystallize either as $I_3In(PPh_3)$ alone, or as an equimolar mixture of $I_3In(PPh_3)$ and $I_3In(PPh_3)_2$ packed in the same unit cell.[42] Similarly for InI_3 and $P(m\text{-Anis})_3$ prepared in cyclohexane, one obtains a mixture that is $\{I_3In[P(m\text{-Anis})_3]\}_{0.97}\cdot\{I_3In[P(m\text{-Anis})_3]_2\}_{0.03}$, but when prepared in ethyl acetate, EA indicates that one obtains a mixture that is $\{I_3In[P(m\text{-Anis})_3]\}_{0.19}\cdot\{I_3In[P(m\text{-Anis})_3]_2\}_{0.81}$.

Because of the relationship between molecular symmetry and NMR parameters, this aspect of the structural analyses is of particular interest. X-ray crystallographic studies of two tetrahedral adducts, $Br_3In[P(p\text{-Anis})_3]$ (Supporting Information) and $I_3In(PPh_3)$,[42] indicate that there is a C_3 axis along the In−P bond, as for $I_3In(PPh_3)$ in $I_3In(PPh_3)_2\cdot I_3In(PPh_3)$.[42] Among the trigonal−bipyramidal adducts, there is a C_3 axis along the P−In−P axis of $I_3In(PPh_3)_2$ in $I_3In(PPh_3)_2\cdot I_3In(PPh_3)$.[42] The two phosphorus sites in each unique $X_3In(PR_3)_2$ molecular unit are distinct for $Cl_3In(PPh_3)_2$ and $Br_3In(PPh_3)_2$, with coplanar indium and chlorine atoms; $Cl_3In[P(p\text{-Anis})_3]_2$ has a similar structure, with a C_2 symmetry axis along an In−Cl bond.

Solid-State ^{115}In NMR. Experimental ^{115}In NMR parameters determined for the triarylphosphine indium trihalide adducts investigated here are listed in Table 1. With the exception of the spectra for $Br_3In[P(o\text{-Anis})_3]$ and $Br_3In[P(m\text{-Anis})_3]$, the breadths of the central ^{115}In NMR transitions ($m_I = 1/2 \rightarrow m_I = -1/2$) for these complexes exceeded 100 kHz at $B_0 = 21.14$ T, precluding the acquisition of NMR spectra of MAS samples.

1:1 Adducts. Simulation of the central transition powder pattern for the ^{115}In NMR spectrum of $Cl_3In(TDP)$, shown in

Table 1. Experimental ^{115}In NMR Parameters

	C_Q/MHz	η_Q	δ_{iso}/ppm	δ_{11}/ppm	δ_{22}/ppm	δ_{33}/ppm	Ω/ppm	κ	α/deg	β/deg	γ/deg
$Cl_3In(TMP)^a$	−165.0 ± 2.0	0.14 ± 0.02	420 ± 30	470 ± 30	431 ± 30	360 ± 30	110 ± 40	0.30 ± 0.10	90 ± 15	0 ± 15	0 ± 10
$Cl_3In(TDP)$	−166.0 ± 2.0	0.28 ± 0.04	400 ± 30	443 ± 30	413 ± 30	343 ± 30	100 ± 40	0.40 ± 0.10	90 ± 15	0 ± 15	0 ± 10
$Cl_3In[P(o\text{-}Anis)_3]\cdot P(o\text{-}Anis)_3$	−122.0 ± 2.0	0.17 ± 0.04	390 ± 30	442 ± 30	387 ± 30	342 ± 30	100 ± 40	−0.10 ± 0.10	90 ± 10	50 ± 25	0 ± 15
$Cl_3In[P(o\text{-}Anis)_3]$	±106.0 ± 2.0	0.60 ± 0.04	400 ± 30	439 ± 30	403 ± 30	359 ± 30	80 ± 40	0.10 ± 0.20	5 ± 10	75 ± 15	50 ± 20
$Cl_3In[P(p\text{-}Anis)_3]_2$	±86.0 ± 2.0	0.35 ± 0.08	300 ± 50	600 ± 50	180 ± 50	120 ± 50	480 ± 70	−0.75 ± 0.20	15 ± 10	85 ± 5	5 ± 5
$Cl_3In[P(m\text{-}Anis)_3]_2$	±54.0 ± 4.0	0.75 ± 0.10	310 ± 30	649 ± 30	182 ± 30	99 ± 30	550 ± 40	−0.70 ± 0.20	0 ± 15	90 ± 15	0 ± 10
$Cl_3In(PPh_3)_2$	±44.0 ± 2.0	0.66 ± 0.04	310 ± 30	622 ± 30	166 ± 30	142 ± 30	480 ± 40	−0.90 ± 0.10	85 ± 5	2 ± 2	12 ± 4
$Br_3In(TMP)$	−166.0 ± 2.0	0.23 ± 0.05	260 ± 40	335 ± 40	290 ± 40	155 ± 40	180 ± 60	0.50 ± 0.20	90 ± 15	0 ± 15	0 ± 10
$Br_3In(TDP)$	−166.0 ± 2.0	0.30 ± 0.05	260 ± 40	338 ± 40	284 ± 40	158 ± 40	180 ± 60	0.50 ± 0.20	90 ± 15	0 ± 15	0 ± 10
$Br_3In[P(o\text{-}Anis)_3]$	±72.0 ± 2.0	0.62 ± 0.06	280 ± 40	370 ± 40	280 ± 40	190 ± 40	180 ± 60	0.00 ± 0.20	88 ± 10	75 ± 15	15 ± 20
$Br_3In[P(p\text{-}Anis)_3]$	±1.25 ± 0.10	0.00	323 ± 5	360 ± 5	305 ± 5	305 ± 5	55 ± 7	−1.00	—	90	0
$Br_3In[P(m\text{-}Anis)_3]$	±5.0 ± 1.0	0.00 ± 0.10	305 ± 5	332 ± 5	292 ± 5	292 ± 5	40 ± 7	−1.00 ± 0.10	—	90	0
$Br_3In(PPh_3)_2$	±32.0 ± 2.0	0.27 ± 0.05	120 ± 30	424 ± 30	−8 ± 30	−56 ± 30	480 ± 40	−0.80 ± 0.10	80 ± 10	40 ± 20	80 ± 20
$I_3In(TMP)$	−150.0 ± 4.0	0.30 ± 0.05	−100 ± 30	83 ± 30	33 ± 30	−417 ± 30	500 ± 40	0.80 ± 0.10	90 ± 15	0 ± 15	0 ± 10
$I_3In(TDP)$	−148.0 ± 2.0	0.25 ± 0.05	−200 ± 30	−17 ± 30	−67 ± 30	−517 ± 30	500 ± 40	0.80 ± 0.10	90 ± 15	0 ± 15	0 ± 10
$I_3In[P(o\text{-}Anis)_3]$	−75.0 ± 2.0	0.30 ± 0.10	−80 ± 30	147 ± 30	−95 ± 30	−293 ± 30	440 ± 40	−0.10 ± 0.10	84 ± 10	65 ± 10	8 ± 10
$I_3In[P(p\text{-}Anis)_3]$	−40.0 ± 4.0	0.15 ± 0.15	−50 ± 40	270 ± 40	21 ± 40	−440 ± 40	710 ± 60	0.30 ± 0.10	78 ± 10	64 ± 20	14 ± 10
$I_3In(PPh_3)^b$	+24.0 ± 2.0	0.00	−115 ± 30	58 ± 30	58 ± 30	−462 ± 30	520 ± 40	1.00	—	0	0
$I_3In(PPh_3)^c$	+36.0 ± 2.0	0.00	−140 ± 50	33 ± 50	33 ± 50	−487 ± 50	520 ± 70	1.00	—	0	0
$I_3In(PPh_3)_2{}^d$	±120.0 ± 4.0	0.00	−450 ± 50	−343 ± 50	−343 ± 50	−663 ± 50	320 ± 70	1.00	—	0	0

[a] From ref 19. [b] Free $I_3In(PPh_3)$. [c] $I_3In(PPh_3)$ in $I_3In(PPh_3)_2\cdot I_3In(PPh_3)$. [d] $I_3In(PPh_3)_2$ in $I_3In(PPh_3)_2\cdot I_3In(PPh_3)$.

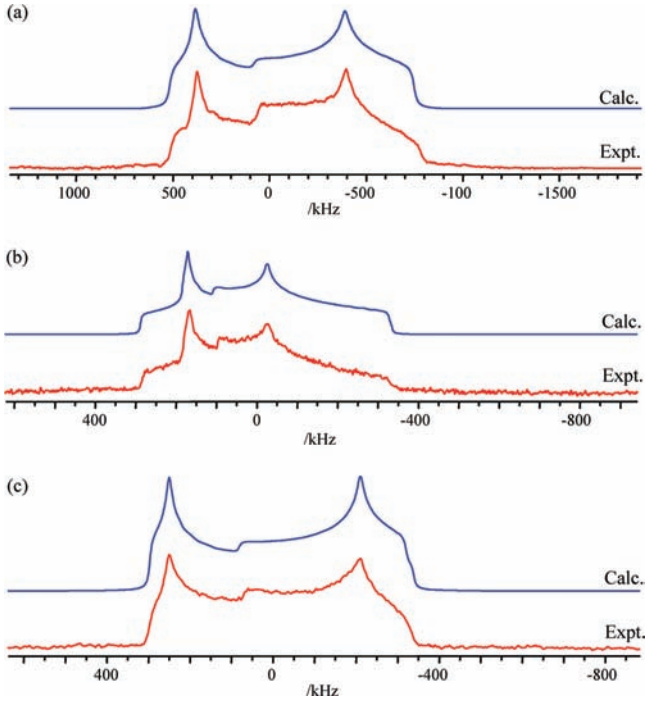

Figure 3. Experimental and calculated ^{115}In NMR spectra of stationary powder samples of (a) $Cl_3In(TDP)$, (b) $Cl_3In[P(o\text{-}Anis)_3]$, and (c) $Cl_3In[P(o\text{-}Anis)_3]\cdot P(o\text{-}Anis)_3$ acquired at 21.14 T.

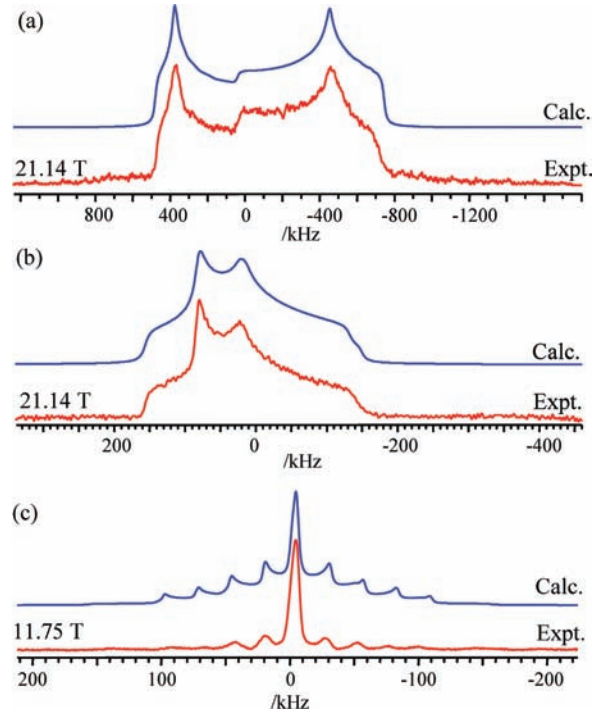

Figure 4. Experimental and calculated central transition powder patterns from ^{115}In NMR spectra of (a) $Br_3In(TMP)$, (b) $Br_3In[P(o\text{-}Anis)_3]$, and (c) from all ^{115}In NMR transitions of $Br_3In[P(p\text{-}Anis)_3]$.

Figure 3(a), yields a $C_Q(^{115}In)$ value of ± 166.0 ± 2.0 MHz, equal, within experimental error, to that for $Cl_3In(TMP)$;[19] the CS tensors for these compounds are also similar. The EFG tensor for the former is almost axially symmetric with V_{ZZ} coincident with δ_{33}; these components are aligned along the approximate C_3 axis. Thus, although crystallographic data for $Cl_3In(TDP)$ are unavailable, these results suggest that the indium coordination environment for this compound must be similar to that for $Cl_3In(TMP)$. The ^{115}In NMR spectra of $Cl_3In[P(o\text{-}Anis)_3]$ and $Cl_3In[P(o\text{-}Anis)_3]\cdot P(o\text{-}Anis)_3$ are shown in Figures 3(b) and 3(c), respectively. The adducts have similar indium CS tensors, but the corresponding EFG tensors are different (Table 1), despite the fact that X-ray crystallography data (Supporting Information) indicate similar environments about the indium. The Euler angles for these adducts suggest that the relative orientations of the EFG and CS tensors are also different, but given the large uncertainties in the spans of the latter, this conclusion must be regarded as tentative. These observations are attributed to the high sensitivity of the indium EFG to minor structural differences, either short or long-range, a consequence of its large nuclear quadrupole moment.

Five $Br_3In(PR_3)$ adducts were examined in this study. Analyses of the ^{115}In NMR spectra for $Br_3In(TMP)$ (Figure 4(a)) and $Br_3In(TDP)$ indicate that these adducts have similar indium EFG and CS tensors (Table 1). The $C_Q(^{115}In)$ value for $Br_3In[P(o\text{-}Anis)_3]$ determined from the ^{115}In NMR spectrum, shown in Figure 4(b), is less than that for $Cl_3In[P(o\text{-}Anis)_3]$. For $Br_3[P(p\text{-}Anis)_3]$, all ^{115}In NMR transitions can be observed—see Figure 4(c). The $C_Q(^{115}In)$ value for this complex, 1.25 ±

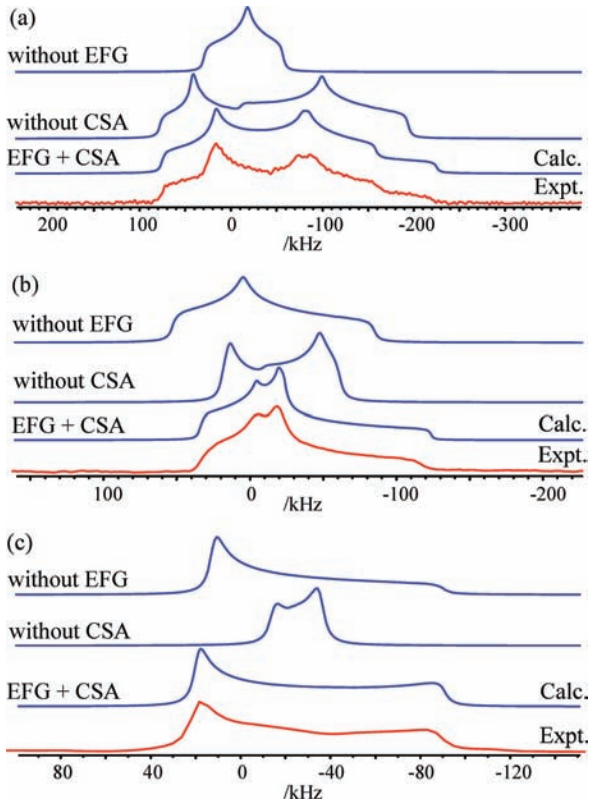

Figure 5. Experimental and calculated ^{115}In NMR spectra of stationary powder samples of (a) $I_3In[P(o\text{-Anis})_3]$, (b) $I_3In[P(p\text{-Anis})_3]$ and (c) $I_3In(PPh_3)$ acquired at 21.14 T. The upper traces show the individual contributions from the indium CSA and EFG.

0.10 MHz, was determined by simulation of all transitions of the ^{115}In NMR spectrum; this value is consistent with a previous prediction based on an analysis of ^{31}P NMR spectra.[27] The asymmetry parameter, $\eta_Q = 0$, and the skew, $\kappa = -1.00$, are also consistent with the crystallographic structure which has a C_3 axis along the In−P bond. Thus, the unique components of the EFG and CS tensors, V_{ZZ} and δ_{11}, respectively, are along the C_3 axis of the molecule. The ^{115}In NMR spectrum for $Br_3In[P(m\text{-Anis})_3]$ (not shown), is similar to that for $Br_3In[P(p\text{-Anis})_3]$; the indium EFG is also very small. Although X-ray data are unavailable for the latter, the values for η_Q and κ suggest that within experimental error, this adduct also has a C_3 symmetry axis along the In−P bond. Since the geometry about the indium for $Br_3In[P(p\text{-Anis})_3]$ is approximately tetrahedral, the small C_Q value suggests that contributions to the EFG from the $P(p\text{-Anis})_3$ ligand are comparable to those from three Br atoms;[58] a similar conclusion seems probable for $Br_3In[P(m\text{-Anis})_3]$, but in this case the structure was not determined.

The indium NMR parameters for the $I_3In(PR_3)$ adducts are also summarized in Table 1. The indium EFG and CS tensors for $I_3In(TMP)$ are similar to those for $I_3In(TDP)$, suggesting that the indium coordination environment for these two adducts are similar, as was found for the indium trichloride and tribromide adducts. Analysis of the ^{115}In NMR spectra for $I_3In[P(o\text{-Anis})_3]$, shown in Figure 5a, indicate that the $C_Q(^{115}In)$ value for this adduct is similar to that for $Br_3In[P(o\text{-Anis})_3]$; that for $I_3In[P(p\text{-Anis})_3]$, shown in Figure 5b, indicates that $C_Q(^{115}In) = -40.0 \pm 4.0$ MHz and $\eta_Q = 0.15 \pm 0.15$.

There is a C_3 symmetry axis along the In−P bond for $I_3In(PPh_3)$ and for $I_3In(PPh_3)$ in $I_3In(PPh_3)_2 \cdot I_3In(PPh_3)$; the η_Q and κ values, 0.0 and 1.00, respectively, indicate that V_{ZZ} and δ_{33} are along the C_3 axis for both adducts. Within experimental error, the values for $C_Q(^{115}In)$ are the only ^{115}In NMR parameters to differ between these two adducts. As for $Cl_3In[P(o\text{-Anis})_3]$ and $Cl_3In[P(o\text{-Anis})_3] \cdot P(o\text{-Anis})_3$ discussed above, this observation is attributed to the high sensitivity of the indium EFG tensors to relatively subtle differences in the environment about the indium (for EFG tensors, long-range effects can have a significant effect).

The indium magnetic shielding anisotropy for the $I_3In(PR_3)$ adducts has a much greater effect on the ^{115}In NMR spectra (Figure 5) than do those for $Cl_3In(PR_3)$ and $Br_3In(PR_3)$. In fact, for spectra acquired at 21.14 T, the contribution from the anisotropy in the indium magnetic shielding for $I_3In[P(p\text{-Anis})_3]$ and $I_3In(PPh_3)$ exceeds that from the second-order term of the indium quadrupolar interaction (Figures 5(b) and 5(c), respectively).

2:1 Adducts. NMR parameters obtained from the simulation of the experimental ^{115}In NMR spectra for the $X_3In(PR_3)_2$ adducts with trigonal−bipyramidal structures, $Cl_3In[P(p\text{-Anis})_3]_2$, $Cl_3In[P(m\text{-Anis})_3]_2$, $Cl_3In(PPh_3)_2$, $Br_3In(PPh_3)_2$ and $I_3In(PPh_3)_2$ in $I_3In(PPh_3)_2 \cdot I_3In(PPh_3)$, are summarized in Table 1; see Figure 6 for some representative spectra. The $C_Q(^{115}In)$ values range from $\pm$ 32.0 $\pm$ 2.0 to $\pm$ 120.0 $\pm$ 4.0 MHz; there is a significant contribution to the ^{115}In NMR spectra from the indium magnetic shielding anisotropy, particularly at 21.14 T. The spans of the 2:1 $InCl_3$ and $InBr_3$ adducts are much greater than those for the corresponding 1:1 adducts. For NMR spectra of $Cl_3In[P(p\text{-Anis})_3]_2$, $Cl_3In[P(m\text{-Anis})_3]_2$, $Cl_3In(PPh_3)_2$ and $I_3In(PPh_3)_2$ acquired at 21.14 T, the anisotropic magnetic shielding is comparable to the second-order quadrupolar perturbation (in frequency units); for the latter, the values η_Q, 0, and κ, 1.00, indicate that V_{ZZ} and δ_{33} are along the C_3 axis. For $Br_3In(PPh_3)_2$, the anisotropic magnetic shielding dominates at higher applied magnetic field strengths.

Summary of ^{115}In NMR Results. The $C_Q(^{115}In)$ values for the indium complexes investigated here cover a wide range, from 1.25 $\pm$ 0.10 to −166.0 $\pm$ 2.0 MHz (Table 1). There is no obvious relationship between $C_Q(^{115}In)$ and the structures of the adducts. A comparison of adducts with the same triarylphosphine ligand indicates that the indium nuclei are most and least shielded for X = I and Cl, respectively, as shown in Figure 7 and summarized in Table 1; this has been attributed to the spin−orbit effect of the halogen ligand.[33] The spans of the indium magnetic shielding tensors for the adducts considered here range from 40 $\pm$ 7 to 710 $\pm$ 60 ppm. For X = Cl or Br, these are greatest for the 2:1 adducts. For the 1:1 adducts, Ω increases as X changes from Cl to I, but for $X_3In(PPh_3)_2$, Ω decreases on going from Cl to I (Figure 7).

Solid-State ^{31}P NMR. The experimental ^{31}P NMR parameters determined for the triarylphosphine indium trihalide adducts are summarized in Table 2. Figures 8−10 provide examples of ^{31}P NMR spectra for several $X_3In(PR_3)$ and $X_3In(PR_3)_2$ adducts. A common feature of the spectra of MAS samples for all adducts, as observed previously,[27] is the unequal relative heights of the peaks in each multiplet, although the integrated intensities of each of the 10 peaks are equal, within experimental error. In particular, the outer peaks associated with the transitions $|1/2,9/2\rangle \rightarrow |-1/2,9/2\rangle$ and $|1/2,-9/2\rangle \rightarrow |-1/2,-9/2\rangle$ are sharper than those associated with indium spin states of $\pm 7/2$. Similar observations have been reported for solution NMR studies (e.g.,

(58) Brill, T. B. *Inorg. Chem.* **1976**, *15*, 2558–2560.

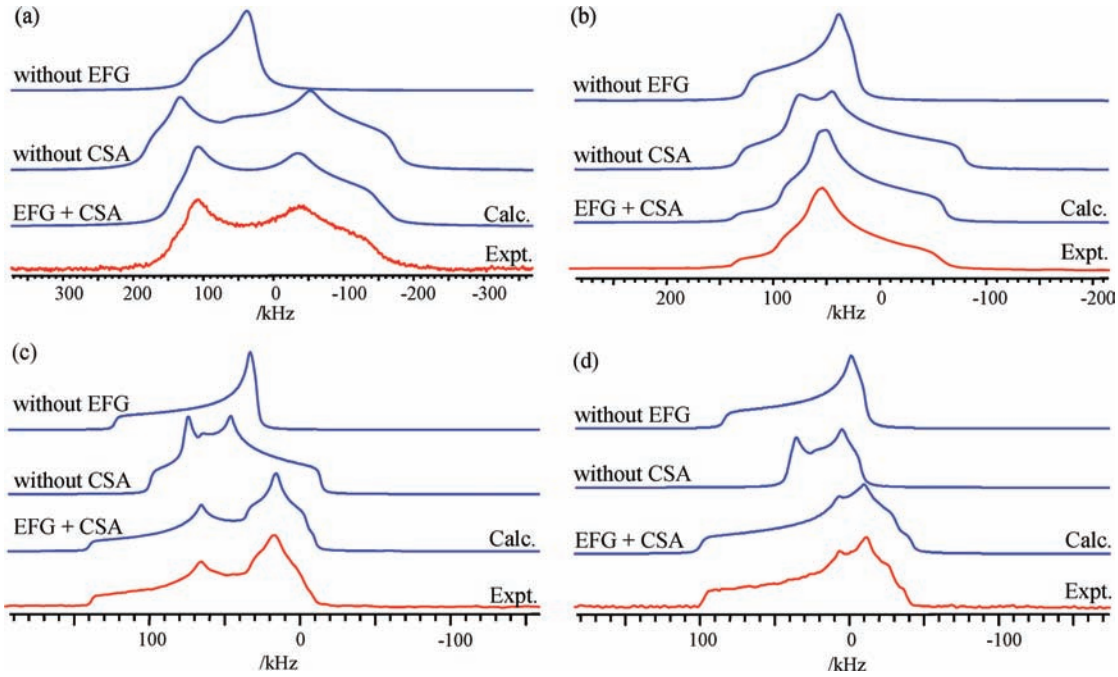

Figure 6. Experimental and calculated ^{115}In NMR spectra of stationary powder samples of (a) $Cl_3In[P(p\text{-Anis})_3]_2$, (b) $Cl_3In[P(m\text{-Anis})_3]_2$, (c) $Cl_3In(PPh_3)_2$ and (d) $Br_3In(PPh_3)_2$ acquired at 21.14 T. The upper traces show the individual contributions from the indium CSA and EFG.

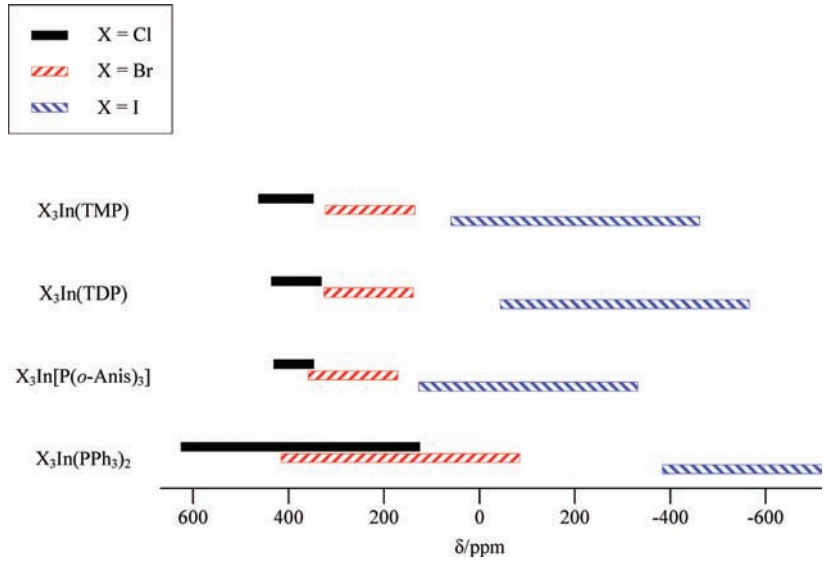

Figure 7. Spans of the CS tensors for the $X_3In(TMP)$, $X_3In(TDP)$, $X_3In[P(o\text{-Anis})_3]$ and $X_3In(PPh_3)_2$.

^{19}F NMR spectra of BiF_6^-, $I(^{209}Bi) = 9/2$;[59] ^{17}O NMR spectra of TcO_4^-, $I(^{99}Tc) = 9/2$),[60] and is attributed to different relaxation rates between the spin states of the coupled quadrupolar nucleus.[61] Expressions for the relative probabilities of single- and double-quantum transitions of spin-9/2 nuclei in the solid state are not known. Spin−spin interactions with quadrupolar nuclei may also give rise to differential broadening of the peaks in the spectra of spin-1/2 nuclei (see Figure S1 and the accompanying text in Supporting Information for a detailed discussion of this effect). However these interactions are not responsible for the patterns seen in Figures 8−10.

The $^1J(^{115}In,^{31}P)$ and $R_{eff}(^{115}In,^{31}P)$ values for the adducts considered here are too small to be extracted from ^{115}In NMR spectra of stationary samples, but as discussed in the theoretical section, one might expect to obtain these parameters from ^{31}P NMR spectra. $^1J(^{115}In,^{31}P)$ can be obtained from an analysis of ^{31}P NMR spectra of MAS samples and $R_{eff}(^{115}In,^{31}P)$ may be obtained from those of either stationary or MAS samples. The latter value along with that for $R_{DD}(^{115}In,^{31}P)$, available from the In−P bond length, may be used to estimate $\Delta J(^{115}In,^{31}P)$ if the **J** and dipolar tensors are coincident with a C_3 symmetry axis along the In−P bond. In such cases, the EFG tensors are axially symmetric with the unique component along the In−P

(59) Morgan, K.; Sayer, B. G.; Schrobilgen, G. J. *J. Magn. Reson.* **1983**, *52*, 139–142.
(60) Buckingham, M. J.; Hawkes, G. E.; Thornback, J. R. *Inorg. Chim. Acta* **1981**, *56*, L41–L42.
(61) Pople, J. A. *Mol. Phys.* **1958**, *1*, 168–174.

Table 2. Experimental ^{31}P NMR Parameters

	δ_{iso}/ppm	δ_{11}/ppm	δ_{22}/ppm	δ_{33}/ppm	Ω/ppm	κ	$R_{eff}(^{115}In,^{31}P)$/Hz	$R_{DD}(^{115}In,^{31}P)$/Hz[a]	$^1J(^{115}In,^{31}P)$/Hz	$\Delta J(^{115}In,^{31}P)$/Hz
$Cl_3In(TMP)$	−49.8 ± 2.0	−22.7 ± 2.0	−60.1 ± 2.0	−66.7 ± 2.0	44.0 ± 3.0	−0.70 ± 0.10	+120 ± 50	+647 ± 20	+2500 ± 20	+1581 ± 200
$Cl_3In(TDP)$	−64.5 ± 2.0	−32.0 ± 2.0	−79.5 ± 2.0	−82.0 ± 2.0	50.0 ± 3.0	−0.90 ± 0.10	+120 ± 50	+636 ± 30[b]	+2410 ± 20	+1548 ± 300
$Cl_3In[P(o\text{-Anis})_3]\cdot P(o\text{-Anis})_3$	−38.5 ± 2.0	−16.9 ± 2.0	−46.7 ± 2.0	−51.9 ± 2.0	35.0 ± 3.0	−0.70 ± 0.20	+120 ± 50	+639 ± 20	+2080 ± 20	+1557 ± 200
	−23.2 ± 1.0	—	—	—	—	—	—	—	—	—
$Cl_3In[P(o\text{-Anis})_3]$	−30.0 ± 2.0	—	—	—	—	—	—	—	+2120 ± 20	—
$Cl_3In[P(p\text{-Anis})_3]_2$	−0.7 ± 1.0	—	—	—	—	—	—	—	+1230 ± 20	—
	−5.8 ± 1.0	—	—	—	—	—	—	—	+1220 ± 20	—
$Cl_3In[P(m\text{-Anis})_3]_2$	−0.2 ± 1.0	—	—	—	—	—	—	—	+1060 ± 20	—
$Cl_3In(PPh_3)_2$	−3.7 ± 1.0	—	—	—	—	—	—	—	+1070 ± 20	—
	−2.3 ± 1.0	—	—	—	—	—	—	—	+940 ± 20	—
$Br_3In(TMP)$	−49.8 ± 2.0	−30.3 ± 2.0	−58.8 ± 2.0	−60.3 ± 2.0	30.0 ± 3.0	−0.90 ± 0.10	+130 ± 50	+631 ± 20	+2220 ± 20	+1503 ± 200
$Br_3In(TDP)$	−59.8 ± 2.0	−39.0 ± 2.0	−69.4 ± 2.0	−71.0 ± 2.0	32.0 ± 3.0	−0.90 ± 0.10	+150 ± 50	+615 ± 30[c]	+2150 ± 20	+1395 ± 300
$Br_3In[P(o\text{-Anis})_3]$	−20.4 ± 1.0	—	—	—	—	—	—	—	+1590 ± 20	—
$Br_3In[P(p\text{-Anis})_3]$	−20.9 ± 0.5	3.1 ± 0.5	−32.9 ± 0.5	−32.9 ± 0.5	36.0 ± 0.7	−1.00	+230 ± 50	+615 ± 20	+1112 ± 20	+1155 ± 150[d]
$Br_3In[P(m\text{-Anis})_3]$	−14.6 ± 1.0	9.4 ± 1.0	−26.6 ± 1.0	−26.6 ± 1.0	36.0 ± 1.5	−1.00	+240 ± 50	+615 ± 30[c]	+1125 ± 20	+1125 ± 300
$Br_3In(PPh_3)_2$	−8.5 ± 0.5	—	—	—	—	—	—	—	+680 ± 20	—
	−6.0 ± 0.5	—	—	—	—	—	—	—	+550 ± 20	—
$I_3In(TMP)$	−59.6 ± 0.5	−40.6 ± 0.5	−67.6 ± 0.5	−70.6 ± 0.5	30.0 ± 0.7	−0.80 ± 0.10	+150 ± 50	+593 ± 30[e]	+1720 ± 20	+1329 ± 300
$I_3In(TDP)$	−68.0 ± 2.0	−43.9 ± 2.0	−78.1 ± 2.0	−81.9 ± 2.0	38.0 ± 3.0	−0.80 ± 0.10	+240 ± 50	+593 ± 30[e]	+1620 ± 30	+1059 ± 300
$I_3In[P(o\text{-Anis})_3]$	−37.2 ± 1.0	−19.5 ± 1.0	−44.7 ± 1.0	−47.5 ± 1.0	28.0 ± 1.5	−0.80 ± 0.10	+220 ± 50	+593 ± 30[e]	+1080 ± 20	+1119 ± 300
$I_3In[P(p\text{-Anis})_3]$	−25.1 ± 1.0	−3.7 ± 1.0	−35.0 ± 1.0	−36.7 ± 1.0	33.0 ± 1.5	−0.90 ± 0.10	+150 ± 50	+616 ± 20	+820 ± 20	+1398 ± 200
$I_3In[P(m\text{-Anis})_3]$[f]	−25.2 ± 1.0	—	—	—	—	—	—	—	+620 ± 20	—
$I_3In(PPh_3)$[g]	−23.5 ± 0.5	−0.8 ± 0.5	−34.8 ± 0.5	−34.8 ± 0.5	34.0 ± 0.7	−1.00	+240 ± 50	+593 ± 20	+680 ± 20	+1059 ± 200
$I_3In(PPh_3)$[h]	−30.0 ± 2.0	—	—	—	—	—	—	—	+620 ± 20	—

[a] Calculated from the In−P bond length according to eq 1. A correction of −2.5% has been applied to R_{DD}, see text. [b] Calculated as described in footnote *a*, assuming that the In−P bond length is equal to that for $Cl_3In[P(o\text{-Anis})_3]$. [c] Calculated as described in footnote *a*, assuming that the In−P bond length is equal to that for $Br_3In[P(p\text{-Anis})_3]$. [d] See ref 27; the sign for the alternative value (see text) in this reference is incorrect. [e] Calculated as described in footnote a, assuming that the In−P bond length is equal to that for $I_3In(PPh_3)$. [f] $I_3In[P(m\text{-Anis})_3]$ in a mixture of $I_3In[P(m\text{-Anis})_3]$ and $I_3In[P(m\text{-Anis})_3]_2$, see text. [g] Free $I_3In(PPh_3)$. [h] $I_3In(PPh_3)$ in $I_3In(PPh_3)_2\cdot I_3In(PPh_3)$.

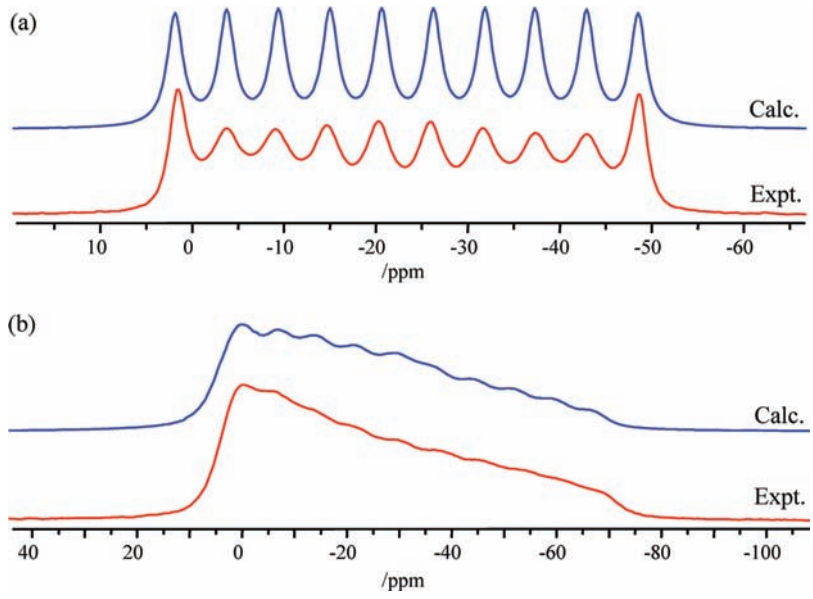

Figure 8. Experimental and calculated ^{31}P NMR spectra of (a) MAS and (b) stationary powder samples of $I_3In(PPh_3)$, acquired at 7.05 T.

bond, $\beta^D = 0$ and $d = (3C_QR_{eff})/(10\nu_S)$ (eq 3). If the sign of $R_{eff}(^{115}In,^{31}P)$ is known, the sign of $C_Q(^{115}In)$ can also be determined. See Table S4 in Supporting Information for a summary of the *d* values. Since the magnitudes of $C_Q(^{115}In)$ for the adducts investigated here were determined from analyses of the ^{115}In NMR spectra, the $R_{eff}(^{115}In,^{31}P)$ values can be determined from the analyses of ^{31}P NMR spectra of MAS or stationary samples. A comparable treatment is possible for molecules possessing an approximate C_3 axis that incorporates the indium nucleus.

When considering errors in experimental values of R_{eff} or R_{DD}, one should be aware that librational effects[62] tend to reduce the direct dipolar interaction; hence values determined from room-temperature NMR measurements are also reduced and yield bond lengths that are larger than those obtained from X-ray or neutron diffraction experiments.[63] Earlier we suggested a correction of 2.5 ± 1.5% to R_{eff} due to librational effects on C−N bonds.[64] Librational effects are expected to be significantly less for In−P bonds than for C−H, N−H or C−N bonds because the former is more rigid. A correction of 2.5%, applied to $R_{DD}(^{115}In,^{31}P)$ values used in the analysis (see below) is thought to be an upper limit to the correction.

As an example, a detailed discussion of the analysis of the data for the 1:1 adduct $I_3In(PPh_3)$ is presented. Analysis of the

(62) Manz, J. *J. Am. Chem. Soc.* **1980**, *102*, 1801–1806.
(63) (a) Ishii, Y.; Terao, T.; Hayashi, S. *J. Chem. Phys.* **1997**, *107*, 2760–2774. (b) Zilm, K. W.; Grant, D. M. *J. Am. Chem. Soc.* **1981**, *103*, 2913–2922.

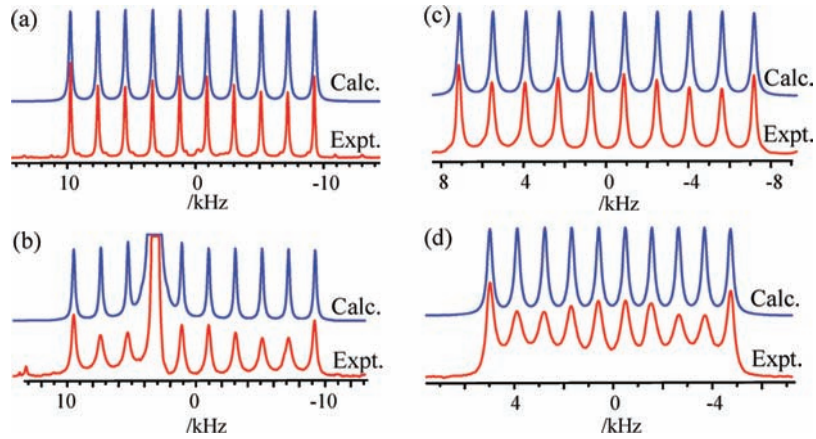

Figure 9. Experimental and calculated ^{31}P NMR spectra of MAS powder samples of (a) $Cl_3In[P(o\text{-Anis})_3]$, (b) $Cl_3In[P(o\text{-Anis})_3]\cdot P(o\text{-Anis})_3$, (c) $Br_3In[P(o\text{-Anis})_3]$ and (d) $I_3In[P(o\text{-Anis})_3]$, acquired at 11.75 T. The peak with the higher intensity seen in (b) is attributed to uncoordinated $P(o\text{-Anis})_3$ in $Cl_3In[P(o\text{-Anis})_3]\cdot P(o\text{-Anis})_3$.

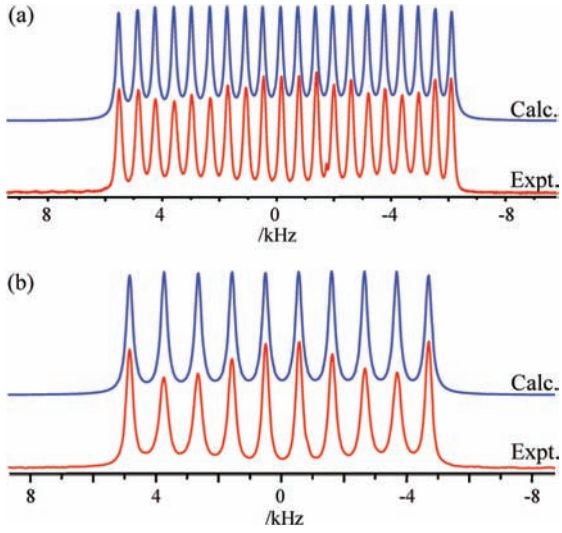

Figure 10. Experimental and calculated ^{31}P NMR spectra of MAS powder samples of (a) $Cl_3In[P(p\text{-Anis})_3]_2$ and (b) $Cl_3In[P(m\text{-Anis})_3]_2$, acquired at 7.05 T.

spectra of MAS and stationary samples (Figure 8) yielded values of 680 ± 20 and 240 ± 50 Hz for $^1J(^{115}In,^{31}P)$ and R_{eff}, respectively. Since there is a C_3 symmetry axis along the In−P bond of this adduct,[42] we may estimate the value for $\Delta J(^{115}In,^{31}P)$ from the relationship $\Delta J = 3(R_{DD} - R_{eff})$. From the known In−P bond length (2.603 Å),[42] an uncorrected value of 608 ± 20 Hz is obtained for R_{DD}; this is reduced to 593 ± 20 Hz after applying the correction for librational motion discussed in the preceding paragraph. Hence, values for ΔJ of +1059 ± 200 or +2499 ± 200 Hz are obtained for ΔJ, depending on the sign of R_{eff}. Since an analysis of ^{31}P NMR spectra of stationary samples showed that $^1J(^{115}In,^{31}P)$ and $R_{eff}(^{115}In,^{31}P)$ have the same sign, and since one-bond spin−spin coupling constants in analogous compounds are positive,[65,66] $^1J(^{115}In,^{31}P)$ and R_{eff} are assumed to be positive;[27,67] thus, the smaller of the two possible values for ΔJ is more probable. $\Delta J(^{115}In,^{31}P)$ and $^1J(^{115}In,^{31}P)$ therefore have similar magnitudes and are both positive. Note that the value for $\Delta J(^{115}In,^{31}P)$ may be considered a minimum, since in the absence of the correction for librational motion, a larger value would be obtained, even if the lesser of the two possible solutions were used. Comparable $\Delta J(^{115}In,^{31}P)$ and $^1J(^{115}In,^{31}P)$ values were also observed for InP.[68] Because the effects of residual dipolar coupling are apparent in ^{31}P NMR spectra of $I_3In(PPh_3)$ acquired with MAS at lower fields, a value for $C_Q(^{115}In)$ had to be included in the analysis, which indicated that $C_Q(^{115}In)$ is positive, consistent with the results obtained from DFT calculations (*vide infra*).

A comparable analysis was performed for $Cl_3In[P(o\text{-Anis})_3]\cdot P(o\text{-Anis})_3$, $Br_3In(TMP)$, $Br_3In[P(p\text{-Anis})_3]$, and $I_3In[P(p\text{-Anis})_3]$; the values for $\Delta J(^{115}In,^{31}P)$ are summarized in Table 2. The analysis outlined in the previous paragraph assumes that the **J** and dipolar tensors are coincident and axially symmetric. With the exception of $Br_3In[P(m\text{-Anis})_3]$, the asymmetry in the indium EFG and shielding tensors for the latter compounds indicate that this may not be the case, but X-ray data (Supporting Information) indicate that these have near C_3 symmetry. The large difference between R_{eff} and R_{DD} must be a consequence of $\Delta J(^{115}In,^{31}P)$, and since the analysis yields comparable values of $\Delta J(^{115}In,^{31}P)$ for closely related adducts, the deviation from axial symmetry is not thought to be sufficient to significantly affect the values obtained. These analyses assumed that the signs of $^1J(^{115}In,^{31}P)$ for these adducts are positive; DFT calculations (*vide infra*) support this assumption. For $Br_3In[P(p\text{-Anis})_3]$, the ten peaks in the ^{31}P MAS NMR spectrum due to the coupling between ^{31}P and ^{115}In are equally spaced, as expected from the $C_Q(^{115}In)$ values of ± 1.25 ± 0.10 MHz determined from an analysis of the ^{115}In spectra; in this case the small value for *d* precludes a determination of a sign for $C_Q(^{115}In)$.

We were unable to obtain X-ray crystallography data for some 1:1 adducts, and thus the value for the In−P bond length was not determined. Examination of the data for other 1:1 adducts

(64) Bryce, D. L.; Wasylishen, R. E. *Inorg. Chem.* **2002**, *41*, 4131–4138.
(65) (a) Nöth, H.; Wrackmeyer, B. *NMR Basic Princ. Prog.* **1978**, *14*, 1–462. (b) McFarlane, H. C. E.; McFarlane, W.; Rycroft, D. S. *J. Chem. Soc., Faraday Trans. 2* **1972**, *68*, 1300–1305.
(66) (a) Rudolph, R. W.; Schultz, C. W. *J. Am. Chem. Soc.* **1971**, *93*, 6821–6822. (b) Cowley, A. H.; Damasco, M. C. *J. Am. Chem. Soc.* **1971**, *93*, 6815–6821.
(67) (a) Jameson, C. J. Spin-Spin Coupling. In *Multinuclear NMR*; Mason, J., Ed.; Plenum Press: New York, 1987; Chapter 4, pp 89−131. (b) Jameson, C. J. Theoretical Considerations: Spin-Spin Coupling. In *Phosphorus-31 NMR Spectroscopy in Stereochemical Analysis, Organic Compounds and Metal Complexes*; Verkade, J. G.; Quin, L. D., Eds.; Methods in Stereochemical Analysis, Vol. 8; VCH Publishers, Inc.: Deerfield Beach, FL, 1987; Chapter 6, pp 205−230.
(68) (a) Tomaselli, M.; deGraw, D.; Yarger, J. L.; Augustine, M. P.; Pines, A. *Phys. Rev. B* **1998**, *58*, 8627–8633. (b) Iijima, T.; Hashi, K.; Goto, A.; Shimizu, T.; Ohki, S. *Chem. Phys. Lett.* **2006**, *419*, 28–32.

(Table S2 in Supporting Information) indicates that there is little variation in the In−P bond lengths for a given halide. Hence, values for $\Delta J(^{115}In,^{31}P)$ have been estimated based on the smallest corrected value of R_{DD} (and hence the smallest value for $\Delta J(^{115}In,^{31}P)$) predicted from the In−P bond lengths for a given halide and from the measured R_{eff} values; these are summarized in Table 2.

Phosphorus-31 NMR spectra of MAS samples for several $X_3In(PR_3)$ adducts are shown in Figure 9; the ^{31}P NMR parameters for these are summarized in Table 2. The ^{31}P NMR peaks for $Cl_3In[P(o\text{-Anis})_3]\cdot P(o\text{-Anis})_3$, $Br_3In[P(o\text{-Anis})_3]$ and $I_3In[P(o\text{-Anis})_3]$ are significantly broader than those for $Cl_3In[P(o\text{-Anis})_3]$; this is attributed to the more rapid relaxation of the spin states for the ^{115}In nuclei and has been reported previously for ^{13}C and ^{31}P coupled to ^{59}Co.[24,69] $X_3In(PR_3)$ adducts with values for η_Q of approximately 0 must have an approximate C_3 axis along the In−P bond with V_{ZZ} approximately aligned with this bond (i.e., $\beta^D \approx 0$). In these cases, the signs for $C_Q(^{115}In)$ could be determined from analyses of the ^{31}P MAS NMR spectra; these are listed in Table 1. DFT calculations accurately predicted these signs (*vide infra*).

As expected, the isotropic regions of ^{31}P NMR spectra of $X_3In(PR_3)_2$ adducts with two nonequivalent phosphorus nuclei contain twenty peaks. An interesting example is that for $Cl_3In[P(p\text{-Anis})_3]_2$ acquired at 7.05 T, shown in Figure 10a, which contains 20 approximately equally spaced peaks; if the nuclear magnetic properties of ^{115}In were not known, one might conclude from this spectrum that ^{115}In has a spin quantum number $I = 19/2$! Of course, from the known properties of ^{115}In, it is apparent that this unusual pattern is a consequence of the fortuitous overlap of the peaks from two distinct ^{31}P NMR sites, with a chemical shift difference (in Hz) between them of either $0.5(^1J(^{115}In,^{31}P))$ or $10(^1J(^{115}In,^{31}P))$. Analysis of ^{31}P NMR spectra acquired at different magnetic fields indicates that the former is the case (i.e., every second peak in Figure 10a is assigned to one ^{31}P site coupled to ^{115}In); the slight differential broadening of the peaks, discussed above, is consistent with this assignment. The observation of two distinct ^{31}P NMR sites for this adduct is contrary to what is expected from the X-ray diffraction data, which indicates that the two phosphorus atoms are related by C_2 symmetry and hence should have identical δ_{iso} values. The single crystal observed *via* X-ray diffraction included a methylene chloride molecule of solvation (see Supporting Information), but there is no indication of its presence in the EA data. Hence, the methylene chloride is thought to have been lost from the sample during its preparation for the EA and NMR analyses. The solid-state structure of the sample analyzed by ^{31}P NMR is clearly different from that observed by X-ray diffraction.

Elemental analysis indicates that the molecular formula of the adduct formed by $InCl_3$ and $P(m\text{-Anis})_3$ is $Cl_3In[P(m\text{-Anis})_3]_2$. Although single-crystal X-ray diffraction data for this adduct are unavailable, the presence of only 10 peaks in the ^{31}P NMR spectrum of an MAS sample (Figure 10b) indicates that the two ^{31}P nuclei must be crystallographically equivalent, or very nearly so. The $^1J(^{115}In,^{31}P)$ values for the two ^{31}P sites of $Cl_3In(PPh_3)_2$ and $Br_3In(PPh_3)_2$ are also summarized in Table 2. Since the indium EFG tensors for the $X_3In(PR_3)_2$ adducts (Table 1) are not axially symmetric, there is no C_3 axis along the P−In−P bond, and thus we cannot assume that $\beta^D \approx 0$. Hence, signs for $C_Q(^{115}In)$ could not be determined for these adducts.

Investigators have reported relationships between the electron-donating ability of phosphines and various molecular properties.[70] For example, early studies found a relationship between the base strength of phosphines toward BH_3 and $^1J(^{31}P,^{11}B)$;[66] a similar relationship has also been reported between $^1J(^{199}Hg,^{31}P)$ and the basicity of the phosphine ligand.[71] Wada and Higashizaki found that the basicity of triarylphosphines increases with the level of methoxy substitution.[72] Hence, the basicity of the ligands considered in this study is expected to increase according to: $PPh_3 < P(o\text{-Anis})_3 \approx P(m\text{-Anis})_3 \approx P(p\text{-Anis})_3 <$ TDP < TMP. For the adducts investigated here, the $^1J(^{115}In,^{31}P)$ values generally increase in the same order. Relationships between one-bond spin−spin coupling and the nature of the bond between the nuclei of interest have been explained by the assumption that the former is dominated by the Fermi-contact mechanism;[73] this conclusion is consistent with the results of DFT calculations for the adducts investigated here (*vide infra*). However, one must consider that the Fermi contact term contributes only to J_{iso};[36,37] the observation of $\Delta J(^{115}In,^{31}P)$ for several of these adducts indicates that mechanisms other than the Fermi-contact term also make significant contributions to the In−P **J** tensor.[27,37]

Summarizing, $^1J(^{115}In,^{31}P)$ values have been determined for all $X_3In(PR_3)$ and $X_3In(PR_3)_2$ adducts investigated here. In addition, when sufficient data were available, $\Delta J(^{115}In,^{31}P)$ values were estimated, and signs for this parameter and for $^1J(^{115}In,^{31}P)$ were proposed. The $^1J(^{115}In,^{31}P)$ and $\Delta J(^{115}In,^{31}P)$ values reported here are of comparable magnitude and positive. Signs for $C_Q(^{115}In)$ have also been determined for those adducts that have high-order symmetry and for which the residual dipolar coupling was observable.

DFT Calculation of ^{115}In EFG Tensors. Calculated ^{115}In EFG tensors are summarized in Table 3; a comparison of experimental and calculated C_Q values is shown in Figure 11. Although some calculated values deviate significantly from the corresponding experimental values, the sign for C_Q was accurately predicted for those samples for which it was determined experimentally. Hence, these results suggest that the experimental procedure used here reliably predicts the sign for $C_Q(^{115}In)$. The calculated η_Q values are also qualitatively in agreement with experiment, as are the calculated relative orientations between the EFG and CS tenors, defined by the Euler angles α, β, γ (Tables 1 and 3).

DFT Calculation of Indium CS Tensors. Because an absolute magnetic shielding scale for indium has not been established, to compare calculated and experimental indium CS tensors, the calculated indium magnetic shielding value for $In(acac)_3$, 3840 ppm, was arbitrarily set to its experimental value, $\delta_{iso}(In) = 35$ ppm;[19] all other calculated magnetic shielding values were converted to chemical shifts according to $\delta_{iso}(In) = 3840 - \sigma_{iso}(In)$, see Tables 3 and 4. Plots of experimental versus calculated $\delta_{iso}(In)$, κ, and Ω are shown in Figure 12; these indicate that calculated CS parameters are qualitatively in

(69) Schurko, R. W.; Wasylishen, R. E.; Nelson, J. H. *J. Phys. Chem.* **1996**, *100*, 8057–8060.

(70) Kühl, O. *Coord. Chem. Rev.* **2005**, *249*, 693–704.

(71) (a) Allman, T.; Goel, R. G. *Can. J. Chem.* **1984**, *62*, 615–620. (b) Allman, T.; Goel, R. G. *Can. J. Chem.* **1984**, *62*, 621–627.

(72) Wada, M.; Higashizaki, S. *J. Chem. Soc., Chem. Commun.* **1984**, 482–483.

(73) Chen, F.; Oh, S.-W.; Wasylishen, R. E. *Can. J. Chem.* **2009**, *87*, 1090–1101.

Table 3. Calculated ^{115}In NMR Parameters

	C_Q/MHz[a]	η_Q	σ_{iso}/ppm	σ_{dia}/ppm	σ_{para}/ppm	$\sigma_{spin-orbit}$/ppm	δ_{iso}/ppm[b]	δ_{11}/ppm	δ_{22}/ppm	δ_{33}/ppm	Ω/ppm	κ	α/deg	β/deg	γ/deg
In(acac)$_3$	+97.3	0.21	3875	—	—	—	−35	4	−49	−59	63	−0.67	57	86	0
Cl$_3$In(TMP)	−112.3	0.17	3394	4899	−2086	581	446	473	453	412	61	0.36	75	17	15
Cl$_3$In[P(*o*-Anis)$_3$]·P(*o*-Anis)$_3$	−63.0	0.51	3401	4891	−2083	593	439	466	438	414	52	−0.08	81	49	5
Cl$_3$In[P(*o*-Anis)$_3$]	−42.5	0.86	3390	4891	−2094	593	450	494	454	402	92	0.13	4	87	39
Br$_3$In(TMP)	−124.8	0.13	3615	4895	−2180	900	225	118	68	−111	229	0.56	77	23	26
Br$_3$In[P(*o*-Anis)$_3$]	−41.6	0.37	3596	4895	−2225	926	244	318	258	155	163	0.26	84	57	26
Br$_3$In[P(*p*-Anis)$_3$]	+27.5	0	3526	4897	−2299	928	314	362	290	290	72	−1.00	90	90	0
I$_3$In[P(*p*-Anis)$_3$]	−20.0	0.04	4031	4896	−2407	1542	−191	83	75	−732	815	0.98	58	19	21
I$_3$In(PPh$_3$)	+67.5	0	4135	4897	−2386	1624	−295	−3	−3	−880	877	1.00	0	0	0
Cl$_3$In(PMe$_3$)$_2$[c]	+82.2	0.14	3532	4895	−1970	607	308	733	124	67	666	−0.83	8	82	1
Cl$_3$In(PMe$_3$)$_2$[d]	−46.4	0.83	3456	4892	−2031	595	384	772	218	163	609	−0.82	87	88	4
Br$_3$In(PMe$_3$)$_2$[e]	−89.2	0.26	3684	4896	−2093	881	156	467	26	−25	492	−0.79	55	86	4
I$_3$In(PMe$_3$)$_2$[f]	+89.1	0	4412	4897	−2138	1653	−572	−445	−445	−827	382	1.00	0	0	0

[a] Calculated C_Q values have been scaled by a factor of 0.951 to correspond to a more recent reported value for Q,[9] see text. [b] δ_{iso}(In)/ppm = 3840 − σ_{iso}(In)/ppm, see ref 19. [c] The structure for the Cl$_3$InP$_2$ core is that for Cl$_3$In[P(*p*-Anis)$_3$]$_2$. [d] The structure for the Cl$_3$InP$_2$ core is that for Cl$_3$In(PPh$_3$)$_2$. [e] The structure for the Br$_3$InP$_2$ core is that for Br$_3$In(PPh$_3$)$_2$. [f] The structure for the I$_3$InP$_2$ core is that for I$_3$In(PPh$_3$)$_2$.

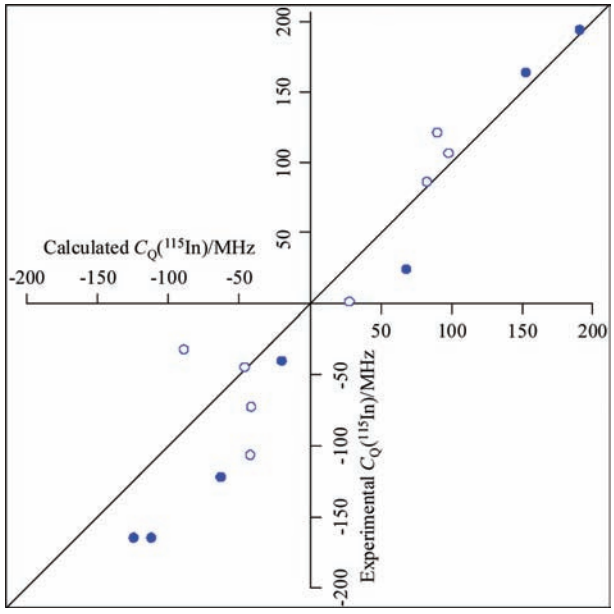

Figure 11. Experimental vs calculated C_Q(^{115}In) values for the triarylphosphine indium trihalide adducts listed in Table 3, as well as for previously reported[19] In(trop)$_3$ and I$_3$In[OP(CH$_3$)$_3$]$_2$ (the two points in the upper right); the diagonal line designates perfect agreement between experimental and calculated values. The solid circles indicate points where the sign for C_Q was determined experimentally; those with open circles are points where the sign was assumed to be that of the calculated value. With this assumption, the standard deviation ($s = [\sum(\text{calc} - \exp)^2/(n-1)]^{1/2}$ where n is the number of data points) is 38 MHz.

agreement with the corresponding experimental values. The experimental trends for δ_{iso}(In) and Ω for X$_3$In(PR$_3$) and X$_3$In(PR$_3$)$_2$, shown in Figure 7, are reproduced in the calculated results listed in Table 3; in particular, the calculated spans for the indium CS tensors of the 1:1 adducts increase from X = Cl to X = I, but the latter has the smallest span for the trigonal−bipyramidal structures. To investigate the causes of the observed trend in the indium magnetic shielding, the diamagnetic, paramagnetic, and spin−orbital contributions to the indium isotropic magnetic shielding were calculated (Table 3). These indicate that as X changes from Cl to I, the diamagnetic term is virtually constant and the paramagnetic term decreases, but the spin−orbital term makes the greatest contribution to the increased magnetic shielding and is the most variable, accounting for the halogen effect[33] discussed above. Trends in the experimental indium CS tensors (Figure 7) are also reproduced by the calculated values for the model 1:1 X$_3$In(PMe$_3$) and 2:1 X$_3$In(PMe$_3$)$_2$ (X = Cl, Br or I) adducts, as shown in Figure 13 and summarized in Table 4.

The increasing indium isotropic shielding for the In(III) complexes with increasing halogen atomic number (normal halogen dependence) is in contrast to what has been observed for InX monohalides, where the shielding decreases, a result that is consistent with DFT calculations (Table S4 of Supporting Information). The latter, referred to as the inverse halogen dependence, IHD, has been reported for B-, Al-, and Ga-halides, where the metal is in the +1 oxidation state.[74] Kaupp and coworkers have undertaken DFT calculations of heavy atom effects on nuclear magnetic shielding.[75] The IHD of the isotropic chemical shifts for the monohalides is a consequence primarily of the far greater deshielding effect of the paramagnetic term, but the trend in the spin−orbit term is also opposite to that for the In(III) adducts, decreasing as the halogen atomic number increases.

DFT Calculations of ^1J(^{115}In,^{31}P) and ΔJ(^{115}In,^{31}P). The calculated ^1J(^{115}In,^{31}P) and ΔJ(^{115}In,^{31}P) values for the Cl$_3$In(PR$_3$) and Br$_3$In(PR$_3$) adducts, as well as their signs, are listed in Table 5. These values differ from those measured experimentally but qualitatively reproduce their experimental trends. Specifically, calculated ^1J(^{115}In,^{31}P) and ΔJ(^{115}In,^{31}P) values are of similar magnitudes and are positive, in agreement with experimental results. In addition, the correlation between the ^1J(^{115}In,^{31}P) values and the basicity of the triarylphosphine ligands of Cl$_3$In(PR$_3$) and Br$_3$In(PR$_3$) is reproduced by calculations. The calculated contribution to ^1J(^{115}In,^{31}P)$_{iso}$ from the Fermi-contact mechanism for these model adducts is about 99%, in agreement with the assumption that this mechanism dominates. Calculations also indicate nonzero ΔJ(^{115}In,^{31}P) values; these values are mainly due to the spin−dipolar Fermi-contact (SD × FC) cross term; the contribution of this term to ΔJ(^{115}In,^{31}P) is also about 99%. Thus, both Fermi-contact and spin−dipolar Fermi-contact mechanisms make important con-

(74) Gee, M.; Wasylishen, R. E. Aluminum Magnetic Shielding Tensors and Electric Gradients for Aluminum(I) Hydride, Aluminum(I) Isocyanide, and the Aluminum(I) Halides: Ab Initio Calculations. In *Modeling NMR Chemical Shifts. Gaining Insights into Structure and Environment*; Facelli, J. C., de Dios, A. C., Eds.; ACS Symposium Series 732; American Chemical Society: Washington, DC, 1999; Chapter 19, pp 259−276.

(75) (a) Kaupp, M.; Malkina, O. L.; Malkin, V. G.; Pyykkö, P. *Chem.−Eur. J.* **1998**, *4*, 118–126. (b) Kaupp, M.; Malkina, O. L.; Malkin, V. G. *Chem. Phys. Lett.* **1997**, *265*, 55–59.

Table 4. Calculated Indium NMR Parameters for Model 1:1 $X_3In(PMe_3)$ and 2:1 $X_3In(PMe_3)_2$ (X = Cl, Br, and I) Adducts

	σ_{iso}/ppm	σ_{dia}/ppm	σ_{para}/ppm	$\sigma_{spin-orbit}$/ppm	δ_{iso}/ppm[a]	δ_{11}/ppm	δ_{22}/ppm	δ_{33}/ppm	Ω/ppm	κ
$Cl_3In(PMe_3)$	3292	4895	−2198	595	548	613	515	515	98	−1.00
$Br_3In(PMe_3)$	3526	4897	−2297	928	314	361	290	290	71	−1.00
$I_3In(PMe_3)$	4183	4898	−2418	1703	−343	−102	−102	−825	723	1.00
$Cl_3In(PMe_3)_2$	3438	4893	−2046	591	402	782	212	212	570	−1.00
$Br_3In(PMe_3)_2$	3677	4896	−2091	872	163	498	−5	−5	503	−1.00
$I_3In(PMe_3)_2$	4037	4895	−2196	1338	−197	−142	−142	−306	164	1.00

[a] $\delta_{iso}(In)/ppm = 3840 - \sigma_{iso}(In)/ppm$, see ref 19.

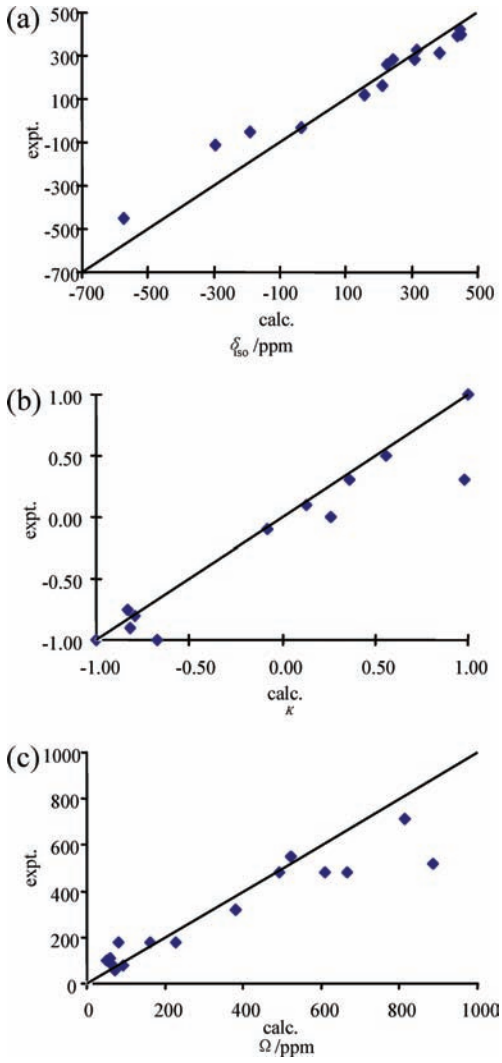

Figure 12. Experimental vs calculated indium CS tensor values (a) δ_{iso}, (b) κ, and (c) Ω for the triarylphosphine indium trihalide adducts $X_3In(PR_3)$ and $X_3In(PR_3)_2$; the diagonal line indicates perfect agreement between experimental and calculated results. The standard deviations (see the caption to Figure 11) are 96 ppm, 0.2, and 123 ppm for δ_{iso}, κ, and Ω, respectively.

tributions to the **J** tensors between coupled indium and phosphorus nuclei.

Conclusions

A series of triarylphosphine indium trihalide adducts, $X_3In(PR_3)$ and $X_3In(PR_3)_2$ (X = Cl, Br or I, PR_3 = triarylphosphine ligand), have been investigated using solid-state ^{115}In and ^{31}P NMR spectroscopy and single-crystal X-ray diffraction. To complement the experimental results, relativistic density functional theory (DFT) calculations have also been performed. The $C_Q(^{115}In)$ values for these adducts range from $\pm 1.25 \pm 0.10$ to -166.0 ± 2.0 MHz; the signs of $C_Q(^{115}In)$ for some adducts with an exact or approximate C_3 axis were determined from analyses of the ^{31}P NMR spectra. For any given phosphine ligand, the indium nuclei are most shielded for X = I and least shielded for X = Cl, a trend also observed for other group-13 elements in the +3 oxidation state. The anisotropic indium magnetic shielding is measurable for all adducts, with spans as large as 710 ± 60 ppm. For adducts with X = I or possessing trigonal−bipyramidal structures, Ω values are significant; at 21.14 T, the contribution of anisotropic shielding to the ^{115}In NMR spectra is of the same magnitude as the contribution from $C_Q(^{115}In)$. $^1J(^{115}In,^{31}P)$ values were determined for all adducts investigated here; $\Delta J(^{115}In,^{31}P)$ values and their signs were also determined for several of these. The $^1J(^{115}In,^{31}P)$ and $\Delta J(^{115}In,^{31}P)$ values are comparable in magnitude and positive. The former generally increase with increasing basicity of the triarylphosphine ligands for $X_3In(PR_3)$ and $X_3In(PR_3)_2$ for any given X.

Theoretical calculations qualitatively reproduce the available experimental ^{115}In EFG and CS tensors, including their relative orientations. The theoretical calculations also reproduce the observed relationship between the isotropic indium magnetic shielding and the halogen ligands, attributed to the spin−orbital effect of the halogen ligand. Calculated values of $^1J(^{115}In,^{31}P)$ and $\Delta J(^{115}In,^{31}P)$ are significantly lower than the experimental values; however, calculations undertaken for the $Cl_3In(PR_3)$ and $Br_3In(PR_3)$ adducts confirm that $^1J(^{115}In,^{31}P)$ and $\Delta J(^{115}In,^{31}P)$ are comparable in magnitude with positive signs and reproduce the apparent relation between $^1J(^{115}In,^{31}P)$ and the basicity of the triarylphosphine ligands. Calculations indicate that both the Fermi-contact and spin−dipolar Fermi-contact mechanisms are important factors when considering the **J** tensor between coupled indium and phosphorus nuclei; however, J_{iso} values are governed by the efficiency of the Fermi-contact mechanism.

The present study has provided an interpretation of solid-state ^{115}In NMR spectra for general indium−phosphine complexes. Analyses of these spectra allowed the determination of indium quadrupolar and CS tensors. Our study has shown that the effect of indium magnetic shielding anisotropy cannot be ignored when interpreting ^{115}In NMR spectra, particularly for spectra acquired at high magnetic-field strengths. We also have demonstrated that relativistic DFT calculations are helpful in the analysis of ^{115}In NMR spectra. In addition, NMR investigations of spin-1/2 nuclei such as ^{31}P coupled to indium complement ^{115}In NMR data; these can yield important NMR information, such as $^1J(^{115}In,^{31}P)$, $\Delta J(^{115}In,^{31}P)$, and the signs for $\Delta J(^{115}In,^{31}P)$ and $C_Q(^{115}In)$, which are difficult or impossible to determine from the analyses of the experimental ^{115}In NMR spectra, and they may also provide estimates of C_Q, corroborating conclusions reached from analyses of the ^{115}In NMR spectra. Finally, this study clearly demonstrates the advantages of

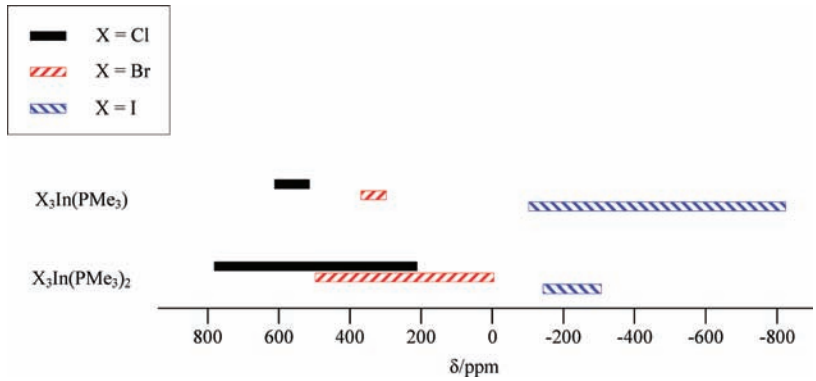

Figure 13. Calculated spans for the indium CS tensors for model adducts.

Table 5. Calculated $^{1}J(^{115}In,^{31}P)$ and $\Delta J(^{115}In,^{31}P)$ Values for $X_3In(PR_3)$ (X = Cl and Br) Adducts

	$^{1}J(^{115}In,^{31}P)$/Hz	$\Delta J(^{115}In,^{31}P)$/Hz
$Cl_3In(TMP)$	+1488	+1250
$Cl_3In(TDP)$	+1329	+1183
$Cl_3In[P(o\text{-Anis})_3]$	+1082	+1066
$Cl_3In[P(p\text{-Anis})_3]$	+822	+1033
$Cl_3In(PPh_3)$	+597	+923
$Cl_3In[P(m\text{-Anis})_3]$	+604	+916
$Br_3In(TMP)$	+1225	+1165
$Br_3In(TDP)$	+1042	+1085
$Br_3In[P(o\text{-Anis})_3]$	+708	+951
$Br_3In[P(p\text{-Anis})_3]$	+456	+891
$Br_3In(PPh_3)$	+351	+832
$Br_3In[P(m\text{-Anis})_3]$	+446	+881

performing ^{115}In NMR experiments at the highest possible magnetic field strength.

Acknowledgment. We thank Victor Terskikh and Eric Ye for acquiring some ^{115}In NMR spectra. We acknowledge Klaus Eichele, Gang Wu, and Jason Clyburne for some preliminary ^{31}P NMR work on this project. Access to the 900 MHz NMR spectrometer was provided by the National Ultrahigh-Field NMR Facility for Solids (Ottawa, Canada), funded by the Canada Foundation for Innovation, the Ontario Innovation Trust, Recherche Québec, the National Research Council of Canada, and Bruker BioSpin and managed by the University of Ottawa (www.nmr900.ca). R.G.C. and R.E.W. thank the Natural Sciences and Engineering Research Council of Canada (NSERC) for financial support through the Discovery Grant Program and a Major Resources Support grant. R.E.W. also thanks the Canada Research Chairs program and the University of Alberta for research support.

Supporting Information Available: Elemental analysis results; selected X-ray experimental and structural data, as well as the CIFs, for $Br_3In(TMP)$, $Cl_3In[P(o\text{-Anis})_3]\cdot P(o\text{-Anis})_3$, $Cl_3In[P(o\text{-Anis})_3]$, $Br_3In[P(o\text{-Anis})_3]$, $Cl_3In[P(p\text{-Anis})_3]_2$, $Br_3In[P(p\text{-Anis})_3]$, $I_3In[P(p\text{-Anis})_3]$, $Cl_3In(PPh_3)_2$ and $Br_3In(PPh_3)_2$; summary of *d* values; experimental and computational indium magnetic shielding parameters for InX monohalides; discussion of the differential line broadening of the ^{31}P NMR spectra; and additional ^{115}In and ^{31}P NMR spectra for all adducts. This material is available free of charge via the Internet at http://pubs.acs.org.

JA100625P